HHS Public Access

Author manuscript

Neuron. Author manuscript; available in PMC 2022 January 06.

Published in final edited form as:

Neuron. 2021 January 06; 109(1): 91–104.e5. doi:10.1016/j.neuron.2020.10.003.

A functional topographic map for spinal sensorimotor reflexes

Graziana Gatto[1], **Steeve Bourane**[1,2], **Xiangyu Ren**[1], **Stefania Di Costanzo**[1], **Peter K. Fenton**[1], **Priyabrata Halder**[3], **Rebecca P. Seal**[3], **Martyn D. Goulding**[1,4,*]

[1]Molecular Neurobiology Laboratory, The Salk Institute for Biological Studies, La Jolla, CA 92037, USA.

[2]Université de la Réunion, DéTROI, UMR 1188 INSERM, Sainte Clotilde, La Réunion, 97490, France

[3]Departments of Neurobiology and Otolaryngology, Center for Neural Basis of Cognition, and Pittsburgh Center for Pain Research, University of Pittsburgh School of Medicine, Pittsburgh, PA, 15260, USA

[4]Lead Contact

SUMMARY

Cutaneous somatosensory modalities play pivotal roles in generating a wide range of sensorimotor behaviors, including protective and corrective reflexes that dynamically adapt ongoing movement and posture. How interneurons (INs) in the dorsal horn encode these modalities and transform them into stimulus-appropriate motor behaviors is not known. Here we use an intersectional genetic approach to functionally assess the contribution that eight classes of dorsal excitatory INs make to sensorimotor reflex responses. We demonstrate that the dorsal horn is organized into spatially restricted excitatory modules composed of molecularly heterogeneous cell types. Laminae I/II INs drive chemical itch-induced scratching; laminae II/III INs generate paw withdrawal movements, and laminae III/IV INs modulate dynamic corrective reflexes. These data reveal a key principle in spinal somatosensory processing, namely, sensorimotor reflexes are driven by the differential spatial recruitment of excitatory neurons.

Graphical Abstract

*Corresponding author contact: goulding@salk.edu.

AUTHOR CONTRIBUTIONS

Conceptualization: G.G. and M.G.; Investigation: G.G., S.B., X.R., S.D.C., P.K.F and P.H.; Resources: R.P.S; Writing – Original Draft: G.G. and M.G.; Writing – Review & Editing: G.G. and M.G.; Visualization: G.G.; Supervision: G.G. and M.G.; Funding Acquisition: M.G.

DECLARATION OF INTERESTS

The authors declare no competing financial interests.

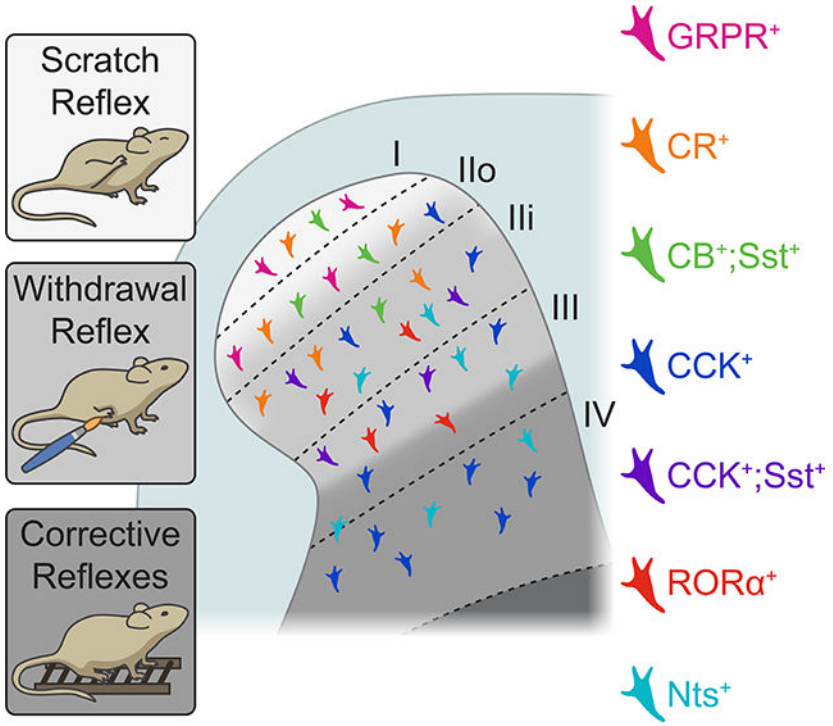

INTRODUCTION

The cutaneous somatosensory system detects a variety of sensory modalities including touch, temperature, pain and itch, which are processed by circuits in the dorsal horn of the spinal cord and medulla (Abraira and Ginty, 2013; Braz et al., 2014; Gatto et al., 2019; Han and Dong, 2014; Jenkins and Lumpkin, 2017; Moehring et al., 2018). These sensory modalities are used to generate a range of sensorimotor behaviors including protective and corrective motor reflexes (Rossignol et al., 2006). How cutaneous sensory information is encoded centrally to generate modality-specific motor reflexes remains unclear. Two divergent views have emerged: one based on the specificity theory of labeled-line transmission (Müller, 1837), and the other on population coding (Melzack and Wall, 1965) that postulates the spatial and temporal coding of sensory inputs as being key in defining the behavioral output (Craig, 2003; Handwerker, 2014; Ma, 2010). While the characterization of many peripheral afferent pathways is consistent with labeled-line transmission (Abraira and Ginty, 2013; Basbaum et al., 2009; Dong and Dong, 2018), other studies point to cross-talk within the spinal cord (Arcourt et al., 2017; Doetsch, 2002; Ma, 2010). However, efforts to deduce the logic of somatosensory coding in the spinal cord are complicated by the high degree of molecular heterogeneity within the dorsal horn (Del Barrio et al., 2013; Häring et al., 2018; Sathyamurthy et al., 2018; Zeisel et al., 2018) and the overlapping input that these molecularly diverse cell types receive as exemplified by the multiple IN classes innervated by low threshold mechanoreceptors (LTMRs) (Abraira et al., 2017). Thus, it still remains to be resolved how molecular heterogeneity in the dorsal horn relates to function and to the organization of the sensorimotor reflex circuitry.

Functional studies to date have largely relied on developmental manipulations that either broadly disrupt large swaths of dorsal excitatory INs resulting in a wide spectrum of sensory deficits (Szabo et al., 2015; Xu et al., 2013), or studies of one or two neuron populations that result in more selective sensory impairments (Abraira et al., 2017; Albisetti et al., 2019; Bourane et al., 2015a; Cheng et al., 2017; Christensen et al., 2016; Duan et al., 2014; Huang et al., 2019; Liu et al., 2018; Paixão et al., 2019; Peirs et al., 2015; Sun and Chen, 2007). Individually these selective studies are suggestive of labeled-line transmission, but when taken together show a multiplicity of IN populations regulating the same response (Albisetti et al., 2019; Christensen et al., 2016; Fatima et al., 2019; Huang et al., 2018; Mishra and Hoon, 2013; Sun and Chen, 2007). Thus, it remains an open question whether these IN populations act as bona fide labeled-lines or function as elements of a broader spinal circuitry that generates stimulus-appropriate sensorimotor responses.

In this study, we have addressed the cellular logic of sensorimotor coding in the dorsal horn by assessing the contribution that eight classes of dorsal excitatory INs make to the spinally driven reflex behaviors. Our analyses reveal that the dorsal horn is organized around sensorimotor reflex modules composed of spatially restricted excitatory networks that are molecularly heterogeneous. We find that multiple excitatory neurons in the superficial dorsal horn (laminae I/II) contribute to the protective scratch reflex, whereas excitatory neuron networks located deeper in laminae II/III drive paw withdrawal reflexes. Finally, excitatory INs that lie deeper still (laminae III/IV) contribute to corrective motor responses. In summary, we propose a functional topographic map of the dorsal horn in which the differential spatial recruitment of excitatory neurons dictates the nature of the sensorimotor reflex.

RESULTS

Sensory-modality specific neuronal activation peaks in distinct laminar patterns

As the first step toward addressing the composition of the spinal networks that encode different sensorimotor responses, expression of the immediate early genes c-Fos and Arc was used to investigate the spatial organization of neurons recruited during scratch and paw withdrawal. Injection of the pruritogen chloroquine into the nape of the neck induced strong c-Fos and Arc expression in laminae I/II at cervical levels (Figures 1A, 1B, S1A and S1B, see also Akiyama et al., 2009; Bell et al., 2016; Gutierrez-Mecinas et al., 2017; Han et al., 2013), similar to what observed following histamine-induced scratching (Figures 1C, 1D and S1C). The recruitment of neurons in laminae I/II is therefore a signature feature of the scratch reflex.

By contrast, mechanical stimuli that elicit paw withdrawal induced ipsilateral c-Fos expression in deeper layers of the dorsal horn (Figures 1E–1H and S1D–S1G), with noxious stimulation of the plantar surface of the hindpaw (pinprick) activating neurons in laminae IIi/III (Figure 1E and 1F) and non-noxious brushing of the paw recruiting neurons in lamina III (Figures 1G and 1H) as previously observed (Bourane et al., 2015a). Together, these results reveal a clear dichotomy between the activity patterns of reflex sensorimotor programs, with superficial neurons being strongly recruited during itch-induced scratching and deep neurons preferentially active during mechanical withdrawal (Figures 1I and 1J).

They also suggest that the neurons driving scratch and paw withdrawal reflexes are organized into spatially distinct sensorimotor modules spanning two or more laminae.

Spatial distribution and molecular identity define distinct spinal microcircuits

Our observation that INs recruited during scratch and paw withdrawal are spatially segregated, led us to test whether excitatory populations that are differently distributed across dorsal horn laminae make specialized contributions to these sensorimotor responses. *Calretinin*^{Cre} (*CR*^{Cre}) targets INs in the more superficial laminae I/II (Duan et al., 2014; Peirs et al., 2015; Petitjean et al., 2019; Smith et al., 2019), whereas *Cholecystokinin*^{Cre} (*CCK*^{Cre}) preferentially captures INs located more deeply in laminae IIi-IV (Abraira et al., 2017; Liu et al., 2018). In support of this, scRNA studies indicate that *CR* and *CCK* mark two largely non-overlapping populations of excitatory neurons (Häring et al., 2018; Sathyamurthy et al., 2018; Zeisel et al., 2018).

When a *Lbx1*^{FlpO} allele was used to circumvent *Cre* expression in the ventral spinal cord, sensory ganglia and motor cortex, excitatory CR^{Cre};Lbx1^{FlpO} INs were seen to be primarily localized to laminae I/II, with only sparse labeling in the other laminae (Figures 2A–2C, S2A and S2C (see also Duan et al., 2014)). By contrast, excitatory CCK^{Cre};Lbx1^{FlpO} INs were largely restricted to the deeper laminae IIi-IV (Figures 2D–2F, S2B and S2C), and did not express CR (Figure S2D–S2F). They did, however, comprise a large fraction of the PKCγ^{+} INs (~33%) that mark laminae IIi and dorsal III (Polgár et al., 1999)), and cMaf^{+} INs (~63%) that are present in laminae III/IV (Del Barrio et al., 2013; Hu et al., 2012) (Figures S2H,S2I, S2K and S2L), with these two markers showing no overlap with the CR^{Cre};Lbx1^{FlpO} INs (Figures S2G, S2I, S2J and S2L), thereby confirming these intersections capture different subsets of dorsal horn excitatory INs. Furthermore, the CR^{Cre} INs located superficially lie within the dorsal horn termination zone for CGRP^{+} afferents (Figure S2M) that transmit nociceptive and pruritic information (Han et al., 2013; Usoskin et al., 2015), whereas the CCK^{Cre} INs spanned the LTMR recipient zone (LTMR-RZ) (Figures S2N and (Abraira et al., 2017)). Consistent with this, monosynaptic rabies tracings showed that small non-mechanosensory (NF200^{-}) CGRP^{+} neurons were presynaptic to the CR^{Cre};Lbx1^{FlpO} but not to the CCK^{Cre};Lbx1^{FlpO} INs (data not shown).

To address whether the differential location of the CR^{Cre} and CCK^{Cre} INs corresponds to different patterns of synaptic output, an AAV2/1-hSyn-DIO-Synaptophysin::phTomato reporter (AAV1-Syp::Tomato) (Figure S2O and (Koch et al., 2017)) was injected unilaterally into the lumbar dorsal horn of *CR*^{Cre} and *CCK*^{Cre} adult mice. CR^{Cre} IN-derived puncta were largely restricted to the ipsilateral superficial dorsal horn (Figures 2I, 2K and 2L) with no puncta detected on motor neurons (Figure S2P). By contrast, ipsilateral and contralateral projections were observed throughout the deep dorsal, intermediate and ventral horn of *CCK*^{Cre} injected animals (Figures 2J–2L), with synaptic puncta present on motor neurons (Figure S2Q) and premotor V2a INs (Figure S2R). Taken together these data argue that *CR*^{Cre}*;Lbx1*^{FlpO} and *CCK*^{Cre}*;Lbx1*^{FlpO} define two spatially distinct populations of dorsal excitatory neurons that are organized into different sensorimotor circuits.

Scratch and withdrawal reflexes are driven by distinct spatially confined excitatory networks

To assess the contribution that each of these two excitatory IN populations make to protective reflexes, we used the intersectional *R26*$^{ds\text{-}hM3D}$ allele (Sciolino et al., 2016) to test whether activating either IN population is sufficient to induce the scratch reflex. CNO-activation of the CR^{Cre};Lbx1^{FlpO} INs, but not the CCK^{Cre};Lbx1^{FlpO} INs, caused a marked increase in spontaneous scratching (Figure 3A). Because the robust scratching elicited by the CR^{Cre};Lbx1^{FlpO} INs would confound any analysis of withdrawal responses, the contribution that these two populations make to paw withdrawal reflexes was instead analyzed by loss-of-function experiments. Ablating the CCK^{Cre};Lbx1^{FlpO} INs, but not the CR^{Cre};Lbx1^{FlpO} INs, caused significant impairments of paw withdrawal to noxious (pinprick, Figure 3B) and non-noxious (brush, Figure 3C) mechanical stimuli. The lack of a paw withdrawal phenotype in the *CR*^{Cre}*;Lbx1*^{FlpO} mice was not due to inefficient cell ablation, as there was a significant loss of INs compared to saline-treated controls (Figures S3A–S3C). Acute inhibition of both cell types using the *R26*$^{ds\text{-}hM4D}$ double stop effector line (Bourane et al., 2015b) phenocopied the ablation-induced behavioral deficits (Figures S3D–S3G), confirming that the loss-of-function phenotypes seen are not due to circuit re-wiring or other plasticity mechanisms.

Activation of the CCK^{Cre};Lbx1^{FlpO} INs resulted in a marked qualitative alteration in the reflex response to pinprick (Figures 3D and S3H and Videos S1–S3), as well as changes in both the frequency of the response and the dynamics of movement following brush stimulation (Figures 3E, 3F and S3I, and Videos S4 and S5). These included holding the paw in a guard position after the initial withdrawal movement (Figures 3D and 3F), and increased lifting of both hindlimbs upon unilateral paw stimulation (Figures S3H and S3I). By contrast, there was no change in the frequency or quality of paw withdrawal when the CR^{Cre};Lbx1^{FlpO} INs were activated (Figures 3D–3F, S3H and S3I). Taken together, our functional analyses suggest that the excitatory neuron networks in the dorsal horn driving scratch and paw withdrawal reflexes are spatially segregated, in line with the differential patterns of neuron activity accompanying these two sensorimotor behaviors (Figure 1I).

Heterogeneous cell types contribute to the chemical itch-induced scratch reflex

Our observation that the chemogenetic activation of CR^{Cre};Lbx1^{FlpO} INs generates spontaneous scratching (Figure 3A), led us to test whether these INs are required for pruritogen-induced scratching. Somewhat surprisingly, ablation of CR^{Cre};Lbx1^{FlpO} INs did not impair the scratch reflex response following chloroquine or histamine injection (Figures S4A and S4B). We then asked whether the apparent lack of any effect on scratching might be due to compensation exerted by other IN types. Calbindin (CB) is expressed in the superficial dorsal horn, where it displays very limited overlap with CR (Chen et al., 2016). We found that CB^{Cre};Lbx1^{FlpO} INs were present throughout laminae I-IV (Figures S4C and S4D), and had limited overlap with the CR^{+} INs as these two markers were for the most part mutually exclusive, when co-expression was measured using a combination of antibody staining and genetics in the developing (Figures 4A–4D) or adult dorsal horn (Figures S4E and S4F). Moreover, pruritogen-driven expression of Arc occurred in CB-negative CR^{Cre};Lbx1^{FlpO} INs and vice versa (Figures S4G and S4H).

In support of the compensation hypothesis, ablating the CB^{Cre};$Lbx1^{FlpO}$ INs reduced chloroquine- and histamine-induced scratching (Figures 4E and 4F). Furthermore, additional parameters associated with the chloroquine-induced scratch response, namely, overall time spent scratching, latency to respond, mean speed and number of movements per scratch episode, were altered in CB^{Cre};$Lbx1^{FlpO}$ IN- but not CR^{Cre};$Lbx1^{FlpO}$ IN-ablated mice (Figures S4I–S4M). Chemogenetic silencing of the CB^{Cre};$Lbx1^{FlpO}$ INs also attenuated the chloroquine-induced scratching (Figure S4N), and reduced c-Fos expression in this IN population (Figures S4O–S4Q), further validating their role in the generation of the scratch reflex.

Paradoxically, activation of the CB^{Cre};$Lbx1^{FlpO}$ INs elicited pronounced grooming instead of scratching (Figure 4G). The resultant CNO-induced expression of c-Fos throughout the dorsal horn (Figures S4R–S4T) suggested that the broad activation of CB^{Cre};$Lbx1^{FlpO}$ INs across several laminae favors grooming over scratching, much like the obsessive grooming behaviors seen in autism mouse models that are thought to be caused by the simultaneous activation of multiple sensorimotor circuits (Orefice et al., 2016). To test this hypothesis, we targeted the superficial subset of CB^{Cre} INs (lamina II) using a Sst^{FlpO} allele (He et al., 2016) (Figures 4H and S4U). The $Tau^{ds\text{-}DTR}$ allele containing a Cre-dependent LacZ reporter that is deleted in cells that express *FlpO* (Britz et al., 2015), was used to confirm that this intersection spares the deep neurons, with LacZ expression persisting in CB^{Cre} INs in laminae III-IV (Figure 4I). Activation of CB^{Cre};Sst^{FlpO} INs produced a pronounced increase in spontaneous scratching (Figure 4J), with no concomitant increase in grooming (Figure S4V). This finding confirms that the superficial CB^{Cre} INs are indeed constituents of the scratch reflex circuitry, and it supports our hypothesis that co-activation of the superficial and deep CB^{Cre} IN populations promotes grooming over scratching. Thus, two non-overlapping populations of superficial excitatory INs, namely the CR^{Cre};$Lbx1^{FlpO}$ INs and CB^{Cre};Sst^{FlpO} INs, contribute to the dorsal horn scratch reflex circuitry.

As a further test of the labeled-line hypothesis in the context of itch-induced scratching, we asked whether the scratch reflex elicited by these two IN populations arises via the common recruitment of neurons in the GRP/GRPR pathway or is instead due to cellular heterogeneity in the spinal scratch circuit. RNAscope was first used to determine whether CR^{Cre};$Lbx1^{FlpO}$ INs in the cervical spinal cord of adult mice express *GRPR* and *GRP*, and if so how many do. 15% of CR^{Cre};$Lbx1^{FlpO}$ INs were found to express *GRPR* (Figures 4K and 4L) and another 9% expressed *GRP* (Figures S4W and S4X), and represented 25% and 23% of the total $GRPR^+$ and GRP^+ INs, respectively (Figures 4L and S4X). To examine if the GRP/GRPR pathway was common to the CR^{Cre};$Lbx1^{FlpO}$ circuit, $CR^{Cre};Lbx1^{FlpO};R26^{ds\text{-}hM3D}$ mice were injected intrathecally either with bombesin-saporin (Bomb-SAP) to ablate the $GRPR^+$ INs (Jensen et al., 2008; Sun et al., 2009) or with unconjugated saporin as a control (Blank-SAP). Bomb-SAP treatment, while able to reduce chloroquine-induced scratching (Figure S4Y), did not abolish spontaneous scratching following CNO-activation of the CR^{Cre};$Lbx1^{FlpO}$ INs (Figure 4M).

Of the CB^{Cre};Sst^{FlpO} INs, 19% expressed *GRP*, representing 21% of the total GRP^+ INs (Figures S4Z and S4AA). GRPR was seen in a minor fraction (5%) of this population (Figures 4N and 4O), accounting for 6% of the total $GRPR^+$ INs. Once again, disrupting the

GRP/GRPR pathway produced no significant reduction in scratching following CNO-activation of $CB^{Cre};Sst^{FlpO}$ INs (Figure 4P), even though scratching responses to chloroquine were significantly reduced (Figure S4AB).

These findings argue that multiple molecularly distinct populations of laminae I/II excitatory INs contribute to the scratch reflex. They appear to do so by differentially influencing the quality of the movement, with the speed of the scratching being dependent on the $GRPR^{+}$ INs but not the $CB^{Cre};Lbx1^{FlpO}$ INs (Figures S4I–S4M and S4AC–S4AG).

Distinct subsets of excitatory INs in laminae II/III cooperate to elicit the withdrawal reflex

Next, we asked if the paw withdrawal reflex is also elicited by a heterogeneous group of excitatory cell types in laminae II/III that display prominent c-Fos expression following brush or pinprick stimulation (Figure 1I). To test this, the Sst^{FlpO} allele was used to capture the dorsal subset of lamina II and dorsal lamina III CCK^{Cre} INs (Figures 5A, 5B and S5A), sparing the deep CCK^{Cre} INs that display persistent LacZ expression from the $Tau^{ds\text{-}DTR}$ reporter (Figure S5B). Paw withdrawal responses to both noxious and non-noxious stimuli were significantly impaired when the $CCK^{Cre};Sst^{FlpO}$ INs were either ablated (Figures 5C and 5D) or silenced (Figures S5C and S5D), demonstrating that the more superficial CCK^{Cre} INs are essential elements of the paw withdrawal reflex circuitry. In support of this, activation of the $CCK^{Cre};Sst^{FlpO}$ INs increased the frequency of paw withdrawal to non-noxious stimulation (Figure S5E), and generated a qualitatively stronger response to pinprick (Figure 5E) and brush (Figure 5F), with mice either holding their paws in guard position (Figures 5E and 5F) or lifting both hindlimbs (Figures S5F and S5G).

Noxious and non-noxious paw withdrawal responses are both affected by manipulations of the $CCK^{Cre};Sst^{FlpO}$ IN population, leading us to hypothesize this might be due to the intersection capturing both laminae IIo and IIi excitatory INs. If true, then manipulations that selectively target laminae IIi/III neurons and exclude lamina IIo neurons should uncouple the noxious and non-noxious withdrawal reflex circuitry. In support of this hypothesis, ablating the $RORα^{Cre};Lbx1^{FlpO}$ INs that are located in laminae IIi/III (Figures 5G and 5H) impaired only the non-noxious paw withdrawal responses (Figures 5I and 5J, see also Bourane et al., 2015a). Conversely, chemogenetic activation of the $RORα^{Cre}$ INs increased the frequency of paw withdrawal responses to light brush from 80% to 100% (Figure 5K), with no increase in guarding or bilateral hindlimb lifting (Figures 5L and S5H) that is likely driven by lamina IIo excitatory INs. Interestingly, the shared impairments of non-noxious paw withdrawal that occur following ablation of $CCK^{Cre};Sst^{FlpO}$ INs and $RORα^{Cre}$ INs are consistent with the idea that the excitatory cell types mediating this reflex are heterogeneous, as the $CCK^{Cre};Sst^{FlpO}$ INs in lamina III show little overlap with the $RORα^{+}$ and $cMaf^{+}$ IN populations (Figures S5I–S5K).

A third population of excitatory INs within the LTMR-RZ expresses *Neurotensin* (*Nts*) (Figure S5L). The $Nts^{Cre};Lbx1^{FlpO}$ intersection recapitulates the Nts antibody pattern (Gutierrez-Mecinas et al., 2019) by primarily targeting neurons in laminae IIi/III (Figures 5M and 5N), including some cells that express $PKCγ^{+}$ (Figures S5M and S5O), but also labels additional lamina IV neurons. Importantly, these $Nts^{Cre};Lbx1^{FlpO}$ INs show little overlap with $RORα^{+}$ INs (Figures S5N and S5O), with *Nts* and *CCK* also labeling different

populations (Gutierrez-Mecinas et al., 2019; Häring et al., 2018). Activating the Nts^{Cre};$Lbx1^{FlpO}$ INs was sufficient to increase the frequency of brush-induced withdrawal responses (Figure 5O), without inducing guarding or the bilateral lifting of the hindlimbs (Figures 5P and S5P). This demonstrates that the Nts^{Cre};$Lbx1^{FlpO}$ INs are also able to drive the paw withdrawal reflex. On the other hand, ablating these INs did not significantly impair the paw withdrawal reflex (Figures 5Q and 5R), which we ascribe to the redundancy in this circuit afforded by other excitatory populations in laminae IIi/III such as the RORα$^+$ and CCK$^+$ INs.

Taken together, these data argue that paw withdrawal responses to non-noxious mechanical stimuli are elicited by different excitatory IN types within the LTMR-RZ. Moreover, we propose that the additional recruitment of excitatory lamina IIo INs during the noxious-driven paw withdrawal reflex adds an aversive component (guarding or bilateral lifting) to the reflex movement.

Excitatory INs that span lamina II determine the threshold of mechanical sensitivity

In view of the contribution that lamina IIo and IIi excitatory INs play in driving noxious versus non-noxious paw withdrawal responses, we asked if the neurons in these laminae cooperate to determine the threshold of tactile sensitivity. To this end, we examined the correlation between changes in mechanical sensitivity and the distribution of each neuron population within the dorsal horn. Our predication was that sensitivity to mechanical stimuli would only be altered by manipulations involving neurons in both laminae IIo and IIi (Figure 6A). As hypothesized, decreases in mechanical sensitivity to graded von Frey filament stimulation only occurred in those intersections where excitatory neurons in both laminae IIo and IIi were lost (*CB^{Cre};$Lbx1^{FlpO}$*; *CR^{Cre};$Lbx1^{FlpO}$*; *CCK^{Cre};$Lbx1^{FlpO}$* and *CCK^{Cre};Sst^{FlpO}*). By contrast, the von Frey threshold remained unchanged when excitatory INs in lamina IIi (*CR^{Cre};Sst^{FlpO}*) or lamina IIo (*$ROR\alpha^{Cre}$;$Lbx1^{FlpO}$* and *Nts^{Cre};$Lbx1^{FlpO}$*) were spared (Figures 6B and S6A). Silencing the CB^{Cre};$Lbx1^{FlpO}$ INs, the CCK^{Cre};$Lbx1^{FlpO}$ INs and the CCK^{Cre};Sst^{FlpO} INs fully recapitulated the aforementioned ablation phenotypes (Figures S6B–S6D). We also confirmed the increased threshold reported for the CR^{Cre};$Lbx1^{FlpO}$ IN-ablated mice (Figure S6E; (Duan et al., 2014)), and the absence of any change when the *$ROR\alpha^{Cre}$* INs were inhibited (Figure S6F).

In support of our hypothesis that excitatory neurons in laminae IIo and IIi act cooperatively to establish biologically appropriate thresholds for paw withdrawal responses, activation of the CB^{Cre};$Lbx1^{FlpO}$, CR^{Cre};$Lbx1^{FlpO}$, CCK^{Cre};$Lbx1^{FlpO}$ and CCK^{Cre};Sst^{FlpO} INs all lowered von Frey thresholds compared to their *FlpO*-negative and saline-treated littermate controls (Figures 6C and S6G). By contrast, activation of the $ROR\alpha^{Cre}$ INs or Nts^{Cre} INs, which are not present in lamina IIo, did not change the von Frey thresholds (Figure 6C).

Excitatory neurons in laminae III/IV encode corrective tactile responses

In addition to stereotypical protective responses, tactile cutaneous stimuli elicit a range of corrective reflexes that are necessary for the dynamic control of ongoing movement (Rossignol et al., 2006). The $ROR\alpha^{Cre}$ INs have essential roles in sensing dynamic touch and generating corrective reflexes during walking (Bourane et al., 2015a), which suggests

these two behaviors might converge onto the same circuit. In light of our observation that somatosensory circuits exhibit a strong laminar organization, we asked whether there are domains within the LMTR-RZ that differentially modulate paw responses and non-noxious stimuli when an animal is either stationary (withdrawal reflex) or locomoting (corrective reflexes).

To examine this issue, we focused on the $CCK^{Cre};Lbx1^{FlpO}$ IN population that spans laminae II-IV. These neurons are innervated by LTMR afferents, but are largely devoid of proprioceptive input (Figures S7A and S7B). A series of skilled motor tasks utilizing beams of different shapes and sizes and an uneven ladder were used to assess their contribution to dynamic corrective reflexes during ongoing locomotion (Figure 7A). In addition to contributing to the stationary paw withdrawal reflexes (Figure 3), the $CCK^{Cre};Lbx1^{FlpO}$ INs were also required for corrective movements during locomotion (Figures 7B, 7C and S7C).

We then assessed the contribution that the superficial and deep subsets of the CCK^{+} IN population make to static and dynamic reflex behaviors. Superficial CCK^{Cre} INs were targeted using the $CCK^{Cre};Sst^{FlpO}$ intersection, whereas the deep CCK^{Cre} INs were targeted using the viral approach described in Peirs et al. 202X. We first assessed the spatial and molecular overlap between these two CCK^{+} subsets by transducing $CCK^{Cre};Sst^{FlpO};R26^{ds\text{-}Tom}$ mice with an AAV8-flex-GFP virus (Figure 7D). Strikingly, these two subsets of CCK^{Cre} INs displayed complementary spatial distribution patterns, with the $CCK^{Cre};Sst^{FlpO}$-labeled Td-Tomato^{+} neurons largely restricted to laminae IIo-III and the virally labeled GFP^{+} neurons primarily located in laminae III/IV (Figure 7E). Most importantly, there was very little overlap (7% of both total GFP^{+} and Td-Tomato^{+} neurons) between both subsets (Figure 7F).

Ablation of the superficial $CCK^{Cre};Sst^{FlpO+}$ INs recapitulated the static paw withdrawal reflex impairments seen when the parental $CCK^{Cre};Lbx1^{FlpO+}$ INs were ablated (Figures 5C–5F and S5C–S5G), while minimally disrupting dynamic corrective reflexes with only the performance in the most challenging task (5 mm circular beam) being impaired (Figures 7G and S7F). Conversely, inhibiting the deep CCK^{Cre} IN subset, using $PSEM^{89S}$-driven silencing following unilateral injection of AAV8-hSyn-Flex-rev-$PSAM^{L141F}$-GlyR-IRES-eGFP (AAV8-GlyR) into the lumbar cord, degraded corrective reflexes on the narrow square beam (Figures 7H and S7H), but failed to impair the static paw withdrawal reflex (Peirs et al. 202X).

As a further test of whether static and dynamic sensorimotor circuits are spatially distinct, we assessed the contribution that the $Nts^{Cre};Lbx1^{FlpO}$ INs make to corrective reflexes given their relative enrichment in the deep laminae (Figure 5N) and lack of a paw withdrawal phenotype to non-noxious stimuli when the mice are stationary (Figure 5R). In support of our hypothesis that dynamic corrective movements are driven by a distinct circuit composed of excitatory neurons located in laminae III/IV, ablating the $Nts^{Cre};Lbx1^{FlpO}$ INs increased the number of slips on both rectangular and circular narrow beams (Figures 7I and S7I). Taken together these results indicate that the circuits for static and dynamic innocuous mechanical reflexes are segregated in the dorsal horn and driven by molecularly heterogeneous excitatory neurons.

DISCUSSION

Our results reveal an underlying cellular logic to the coding of cutaneous sensorimotor behaviors within the dorsal horn, namely that specific somatosensory reflex programs are encoded by spatially restricted dorsal horn modules that comprise heterogenous excitatory cell types. These findings support a model in which functional reflex-specific networks are defined by the spatial organization of their constituent neurons in the dorsal horn.

The dorsal horn modular organization provides the framework for population coding of cutaneous sensorimotor reflexes

The comparative functional analysis reported here provides the broad functional context necessary for understanding how sensorimotor circuits in the dorsal spinal cord are organized at a cellular level. These principles of broad circuit organization were not evaluated in previous studies using developmental mutations that typically cause pleiotropic deficits (Holstege et al., 2008; Rottkamp et al., 2008; Szabo et al., 2015; Villeda et al., 2006; Wang et al., 2013; Xu et al., 2013), or in studies targeting smaller subset of INs (Albisetti et al., 2019; Bourane et al., 2015a; Cheng et al., 2017; Christensen et al., 2016; Duan et al., 2014; Huang et al., 2019; Liu et al., 2018; Mishra and Hoon, 2013; Paixão et al., 2019; Peirs et al., 2015; Sun and Chen, 2007).

We find two non-overlapping IN populations, the $CB^{Cre};Sst^{FlpO}$ and the $CR^{Cre};Lbx1^{FlpO}$ INs (Figures 3A and 4J), contribute to the generation of the scratch reflex independently of the GRP/GRPR pathway (Figures 4M and 4P). While loss-of-function analyses show the CB^{+} (Figures 4E, S4I, S4AD) and $GRPR^{+}$ INs (Mishra and Hoon, 2013; Sun and Chen, 2007) are required for the chemical scratch reflex, the contribution the CR^{+} INs make to this reflex pathway was only revealed by sufficiency experiments (Figure 3A). Other studies also point to additional cell type redundancy in the chemical itch reflex pathway (Fatima et al., 2019; Zhao et al., 2014), with pruritogenic sensory afferents synapsing on molecularly distinct cell types in laminae I/II (Braz et al., 2014; Han et al., 2013; McCoy et al., 2013) and c-Fos activation depicting a heterogeneous landscape of recruited cell types following pruritogen administration (Figures S4G and S4H; Fatima et al., 2019; Gutierrez-Mecinas et al., 2017; Han et al., 2013).

Molecular heterogeneity is also a feature of other reflex modules, with three distinct IN classes, the $CCK^{Cre};Sst^{FlpO}$, $RORα^{Cre};Lbx1^{FlpO}$ and $Nts^{Cre};Lbx1^{FlpO}$ INs, contributing to the paw withdrawal reflex induced by non-noxious stimuli (Figure 5). Static von Frey responses are distributed across the $CR^{Cre};Lbx1^{FlpO}$, $CB^{Cre};Lbx1^{FlpO}$ and $CCK^{Cre};Sst^{FlpO}$ IN populations (Figure 6), while the CCK^{Cre}, $RORα^{Cre};Lbx1^{FlpO}$ and $Nts^{Cre};Lbx1^{FlpO}$ INs collectively drive the corrective reflexes (Figure 7). We propose that distributing this functionality across multiple excitatory cell types ensures that the selection and execution of the sensorimotor reflex is both robust and context-appropriate.

Integration of multiple sensory afferent input generates the appropriate motor response

The ensembles of excitatory neurons within each sensorimotor reflex module which span the termination zones of more than one sensory afferent type (Abraira and Ginty, 2013; Todd,

2010) likely receive a mixture of sensory inputs. This suggests that while the topographic organization of sensory afferent innervation is an important determinant of functionality, it is not the sole determinant. The superficial CR^{Cre} INs receive a significant higher fraction of C-fiber and pruriceptive input (Figures S2M, (Petitjean et al., 2019; Smith et al., 2019; Peirs et al. 202X)), as compared to the deep CCK^{Cre} INs that are preferentially innervated by mechanosensitive afferents (Figures S2N, S7A and S7C (Abraira et al., 2017; Peirs et al. 202X)), which is functionally reflected in their relative contributions to nocifensive versus corrective reflexes. However, additional levels of complexity in the sensory afferent cross-talk are revealed when responses to tactile stimuli are analyzed in greater depth. Ablating the CR^{+} INs reduces von Frey sensitivity (Figure 6B), while sparing the withdrawal reflex (Figures 3B and 3C), which is consistent with the withdrawal reflex requiring a specific combination of LTMR input, as suggested by a prior study showing that the execution of the stereotyped withdrawal movement initiated by $NPY2R^{+}$ Aδ-afferent requires additional Maf^{+} Aβ-LTMR input (Arcourt et al., 2017). The paw withdrawal reflex requires the coordinated activation of lamina II and lamina III excitatory INs (Figure 5), with lamina II excitatory INs regulating the threshold of mechanical sensitivity (Figure 6) and lamina III INs engaging the motor circuitry to drive limb flexion. Manipulations that largely spare lamina III excitatory INs, e.g. CR^{Cre};$Lbx1^{FlpO}$ IN ablation, do not impair the withdrawal reflex (Figure 3), but do affect von Frey-dependent mechanical sensitivity (Figure 6). Conversely, manipulations that primarily target neurons in lamina III but not lamina II, e.g. Nts^{Cre};$Lbx1^{FlpO}$ IN ablation, do not alter the threshold of von Frey sensitivity (Figures 6 and S6). This raises the intriguing hypothesis that the recruitment of neurons in lamina III engages wide-dynamic range (WDR) neurons in the deep dorsal horn (lamina V) that function as reflex encoders to drive flexion movements (Levine et al., 2014; Schouenborg et al., 1995). This conclusion is consistent with previous observations that neuronal manipulations in the superficial dorsal horn which spare lamina III INs are still required for pain coping behaviors but do not affect the acute noxious reflex responses (Huang et al., 2019; Wang et al., 2013).

Our analyses reveal a further subdivision in mechanically driven paw withdrawal responses, with lamina IIo excitatory INs that receive strong HTMR afferent input driving the noxious mechanical withdrawal reflex, while excitatory lamina IIi INs are necessary for paw withdrawal to light touch (Figure 5). We posit that the recruitment of lamina IIo INs provides a pain-like amplification component to the withdrawal response (Figures 3D, 3F, 5E–5F, S3H–S3I and S5J–S5K). Interestingly, paw withdrawal in response to noxious heat was only impaired when the CB^{Cre};$Lbx1^{FlpO}$ INs that span laminae I-IV were ablated (data not shown). By contrast, removing the CR^{Cre};$Lbx1^{FlpO}$ (laminae I/II) or the CCK^{Cre};$Lbx1^{FlpO}$ INs (laminae IIi-IV) had no effect (data not shown). This suggests that acute protective responses to heat may depend on the concomitant activation of excitatory CB^{Cre} INs in lamina I that are innervated by temperature-dedicated sensory afferents (Basbaum et al., 2009) and laminae III/IV INs that receive LTMR input. Taken together these data suggest lamina III INs function as action selector neurons that activate the acute paw withdrawal reflex, as opposed to coping behaviors such as licking or flinching.

Toward an operational definition of dorsal spinal cell types

Considerable effort has been devoted to assessing the molecular heterogeneity within the dorsal horn, either by classical candidate approaches (Del Barrio et al., 2013; Gutierrez-Mecinas et al., 2016) or by unbiased scRNA or snRNA screenings (Häring et al., 2018; Sathyamurthy et al., 2018; Zeisel et al., 2018). While a primary goal of these efforts has been the identification of '*prospective cell types*', how these molecular signatures correlate with function remains to be determined. Our findings suggest that sensorimotor reflexes are encoded by ensembles of dorsal INs bearing multiple molecular signatures as opposed to single restricted molecular cell types. In support of this, we saw no degradation of cutaneous sensorimotor reflexes when more restricted populations were functionally assessed (Figure S6A and data not shown). Likewise, manipulations of sparse excitatory IN populations that are thought to correspond to well-defined cell types, e.g. the $Tac2^{+}$ INs, do not generate discernable sensorimotor reflex deficits (Duan et al., 2014; Mar et al., 2012).

This study provides strong functional evidence for the spatial coding of sensorimotor reflex behaviors, with the sensory information driving these reflexes being distributed over multiple excitatory cell types. The somatosensory system has two major behavioral outputs: acute responses (reflexes) that require the rapid integration and coding of sensory input, and perceptual responses that require accurate representation of the stimulus for adaptive behaviors. Whereas acute reflexes would likely benefit from the convergent actions of multiple cell types that favors velocity over accuracy, perceptual tasks would likely be more reliant on population coding where sensory information is distributed across multiple cell types to maximize the fidelity of the stimulus representation.

Our topographic functional map of the dorsal horn highlights the importance of modularity over molecular heterogeneity for acute reflex responses. Nonetheless, it is intriguing to hypothesize that it may also engender a degree of variability in these seemingly stereotypical sensorimotor reflexes that is context-appropriate, for example, the stumbling corrective reflex (Forssberg, 1979), which is a task-dependent variation of the paw withdrawal reflex. We have found the velocity of scratching is perturbed when the $GRPR^{+}$ INs, but not the CB^{Cre};$Lbx1^{FlpO}$ INs, are inactivated (Figure S4). Likewise performances on the uneven ladder task are affected by manipulations involving the CCK^{Cre};$Lbx1^{FlpO}$ INs but not the $ROR\alpha^{Cre}$;$Lbx1^{FlpO}$ (Bourane et al., 2015a) or the Nts^{Cre};$Lbx1^{FlpO}$ INs (Figure 7). This suggests that smaller IN populations may imbue a degree of variability to stereotypical reflex behaviors.

Our ability to probe cell type heterogeneity within the dI5 excitatory dorsal horn lineage and assess the contribution that developmentally defined cell types make to sensorimotor behaviors has begun to bridge the gap between the early developmental programs that specify cell identity/position and function in the adult. This approach also provides a theoretical framework for understanding the developmental programs that partition the dI5 neuronal lineage into functional excitatory modules comprising of specialized neuronal cell types. Interestingly, the stratification of the dorsal horn into functional layers resembles a key aspect of cortical organization, with position being a primary determinant of function and connectivity. However, in comparison to the cortex, the developmental programs that determine the laminar and cellular organization of the dorsal horn are still poorly

understood. Future efforts to define them will be a necessary step for understanding the organization and functioning of the somatosensory system.

STAR Methods

Resource Availability

Lead Contact—Further information and requests for resources and reagents should be directed to and will be fulfilled by the Lead Contact, Martyn Goulding (goulding@salk.edu).

Materials Availability—All published reagents and mouse lines will be shared upon request within the limits of the respective material transfer agreements.

Data and Code Availability—This study did not generate new datasets or codes.

Experimental Model and Subject Details

Mice were maintained following the protocols for animal experiments approved by the IACUC of the Salk Institute for Biological Studies according to NIH guidelines for animal experimentation. 6- to 8-week old mice of both sexes were used for behavioral experiments. Analysis of the behavioral data showed no gender-bias, with similar responses observed in male and female mice. P5 to 8-week old mice (as indicated in the relative method paragraphs) were used for anatomical and molecular characterization of the spinal INs and for viral tracings. Mice were housed in groups of up to 5 animals on a 12-hour dark/light cycle in a humidity- and temperature-controlled room, and provided with rodent diet (Picolab) and water ad libitum. The following mouse lines were used in this study: *Calbindin*^{Cre} *(CB*^{Cre}*)* was generated by Hongkui Zeng; *Calretinin*^{Cre} *(CR*^{Cre}*)* (Taniguchi et al., 2011); *Cholecystokinin*^{Cre} *(CCK*^{Cre}*)* (Taniguchi et al., 2011); *Chox10::CFP (Chx10*^{CFP}*)* (Crone et al., 2008); *hCdx2::FlpO* (Bourane et al., 2015a); *Lbx1*^{FlpO} (Duan et al., 2014); *Nts*^{Cre} (Leinninger et al., 2011); *R26*$^{Ai14\text{-}Td\text{-}Tomato}$ (Madisen et al., 2010); *R26*$^{Ai65\text{-}ds\text{-}Td\text{-}Tomato}$ (Madisen et al., 2015); *R26*$^{ds\text{-}hM3d}$ (Sciolino et al., 2016); *R26*$^{ds\text{-}hM4d}$ (Bourane et al., 2015b); *R26*$^{ds\text{-}HTB}$ (Stam et al., 2012); *RORα*^{Cre} (Chou et al., 2013); *Sst*^{FlpO} (He et al., 2016)*; Tau*$^{ds\text{-}DTR}$(Duan et al., 2014).

METHODS

Immunohistochemistry—Mice were anesthetized by a single intraperitoneal (i.p.) injection (10 μl/g body weight) of solution containing 10 mg/ml ketamine and 1 mg/ml xylazine immediately prior to perfusion with 20 ml of 4% paraformaldehyde in PBS. Spinal cords were dissected and post-fixed for 1 hr at room temperature (RT), then rinsed 3 times in PBS and cryoprotected in 30% sucrose-PBS overnight at 4° C. Spinal cords were embedded in OCT (Tissue-Tek) and cryosectioned at 20–40 μm using a Leica CM3050 cryostat. Sections were dried at RT and stored at −20° C. Before staining OCT was removed with a 5 min PBS wash. Slides with sections were then incubated in Blocking Solution (PBS, 10% donkey serum and 0.3% Triton X-100) for 1–2 hrs at RT and then incubated with the primary antibody diluted as described in antibody solution (PBS, 1% donkey serum, 0.1% Triton X-100 and 0.025% NaN_3) overnight at 4° C. Sections were then washed 3 times (15 min each) in PBT (PBS and 0.1% Triton X-100) before being incubated for 2 hrs at RT with

antibody solution containing donkey-raised fluorophore–conjugated secondary antibodies (1:1000; Jackson Laboratories). Sections were again washed 3 times (15 min each) in PBT before being mounted with Aqua-Poly/Mount (Polysciences). A Zeiss LSM 700 confocal microscope was used to capture images. ImageJ software was used to count neurons and measure their spatial coordinates using the central canal and dorsal edge of the spinal cord as references. The Cell Count plug-in was used to analyze co-localization. The number of sections per mouse analyzed are 6 for laminar distribution (40 μm) and synaptic output (30 μm), 4–6 for c-Fos staining (30 μm), marker co-localization (20 μm) and rabies tracings (20 μm), 6–8 for RNAscope (14 μm) and 3–4 for cell ablation (40 μm). The Lmx1b antibody was generated in the Goulding lab, following the same protocol described in Kania et al., 2000.

Fluorescent in situ hybridization—Perfusion and tissue preparation were performed as described for immunohistochemistry. 14 μm transverse spinal cord sections of the indicated genotypes were prepared using a Leica Cryostat. Sections were dried at −20° C overnight and then stored at −80° C. Multiple-labeling fluorescent *in situ* hybridization was performed using the RNAscope Multiplex Fluorescent Reagent Kit v2 Assay (Advanced Cell Diagnostic # 323100) following the manufacturer's recommended protocol. We used a mix of three probes: *mm-GRP* revealed with Opal 520 (PerkinElmer), *mm-GRPR* revealed with Opal 650 (PerkinElmer) and *Td-Tomato* revealed with Opal 570 (PerkinElmer). Sections were mounted using ProLong Gold Antifade Mounting Medium with NucBlue Staining (Invitrogen), sealed with nail polish and imaged 14 hrs later at the Zeiss LSM700 confocal microscope using the 40X oil objective.

c-Fos/Arc Induction—For the itch-induced scratch response, P56 mice were injected subcutaneously with chloroquine (200 μg) or histamine (100 μg) in the nape of the neck. The mice were then placed in 10 cm x 10 cm plexiglass boxes. After 60 minutes mice were sacrificed and tissue was collected for analysis. For the brush- and pinprick-induced withdrawal reflex, the plantar surface of the right paw of P56 mice was stimulated for 5 times every 3 minutes for a total of 30 minutes. 60 minutes after the initial stimulation mice were sacrificed and tissue was collected for analysis. This mechanical stimulation protocol did not cause redness or inflammation of the stimulated paw.

Laminar Distribution Analysis—Adult lumbar spinal cord (6- to 8-week old) were cryosectioned at 40 μm. Upon staining with antibodies to Td-Tomato and PKCγ antibodies, sections were imaged at the Zeiss LSM700 confocal microscope using the 20X air objective. Neuron coordinates were recorded with ImageJ. The dorsal edge of the spinal cord was used as origin for the y-axis, and the coordinates of each neurons recorded through each plane of the stack. The y-coordinates were used to assign neurons to the different laminae, whose boundaries were defined using pre-set values based on reference stainings and atlases. To control cords were not smeared or distorted during the sectioning process, each section was stained to identify PKCγ$^+$ INs and verify these neurons were correctly assigned only to laminae IIi and dorsal lamina III. Once the neuron coordinates were recorded, frequency distributions of neurons per lamina were automatically determined using Excel.

Neuronal Ablation—Mice carrying the *CB*^{Cre}*;Lbx1*^{FlpO}, *CR*^{Cre}*;Lbx1*^{FlpO}, *CR*^{Cre}*;Sst*^{FlpO}, *CCK*^{Cre}*;Sst*^{FlpO} and *Nts*^{Cre}*;Lbx1*^{FlpO} alleles in addition to the effector *Tau*$^{ds\text{-}DTR}$ received i.p. injections of diphtheria toxin (DTX, 50 ng/gram of weight; List Biological Laboratories) at P28 and P31, or saline solution in equal volume as control. *CCK*^{Cre}*;Lbx1*^{FlpO}*;Tau*$^{ds\text{-}DTR}$ mice and control *CCK*^{Cre}*;Tau*$^{ds\text{-}DTR}$ received intrathecal injections of diphtheria toxin (DTX, 10 ng; List Biological Laboratories) at P28, P30 and P32. *RORα*^{Cre}*;Lbx1*^{FlpO}*;Tau*$^{ds\text{-}DTR}$ mice received intrathecal injections of diphtheria toxin (DTX, 10 ng; List Biological Laboratories) at P28, P30 and P32, or saline solution in equal volume as control. Intrathecal route was chosen as both *CCK*^{Cre}*;Lbx1*^{FlpO} and *RORα*^{Cre}*;Lbx1*^{FlpO} drove expression of the *DTR* effector in limb muscles.

GRPR^{+} INs were ablated by a single intrathecal injection of bombesin-saporin (400 ng in 10 μL 0.9% sterile saline; Advanced Targeting Systems). Littermate controls of the same genotype received unconjugated saporin (400 ng in 10 μL 0.9% sterile saline; Advanced Targeting Systems). Intrathecal injections were performed as described in (Bourane et al., 2015a).

Intraspinal AAV injection—For AAV8-GlyR and AAV8-flex-GFP, 3-week old mice were anesthetized with 2.5% isoflurane, and an incision along the lumbar skin and muscles was carefully performed until the vertebrae were visible. No laminectomy was performed to minimize trauma. A glass microelectrode with ~50 μm tip or a RN Needle (Hamilton) was inserted on the right dorsal spinal cord between vertebrae at L3-L5 to a depth of −250 μm below the dura, taking care to avoid the posterior spinal arteries. Once the spinal cord was pierced, 1 μl of viral solution was slowly infused over a period of 5 minutes using a picospritzer. For AAV1-Syp::Tomato, 6-week old mice were transduced unilaterally with 500 nl of the virus following a laminectomy to expose the lumbar spinal cord at L4. A RN Needle (Hamilton) was inserted upon piercing the dura and the viral solution was slowly infused using a Hamilton Syringe. For every injection, the needle/capillary was left in place for 2–5 minutes after infusion then slowly removed. The incision was then sutured with stitches (5–0 PDS II).

Rabies Virus Tracing—Focal injections of EnvA-pseudotyped, SADB19-ΔG-mCherry rabies virus (each of 250 nl; ~3.3×10^{10} units per ml) were made bilaterally in the lumbar (L2-L4 segments) dorsal horn of P4-P10 mice expressing the *R26*$^{ds\text{-}HTB}$ allele in homozygosity in combination with the described *Cre/FlpO* alleles. A spinal cord laminectomy was performed at the T13-L1 level while the mice were under 2–3% isoflurane anesthesia, 1–1.5L/min oxygen. After piercing the dura mater, a fine glass capillary was inserted bilaterally on the dorsal spinal cord to inject the virus. The incision was then sutured with stitches (5–0 PDS II). Animals were perfused 5 days post-injection and processed for immunostaining.

Drug Administration—Chloroquine and histamine were dissolved in 0.9% sterile saline and injected subcutaneously in the nape of the neck at a final concentration of 200 μg and 100 μg, respectively. Clozapine-N-oxide (Sigma) was dissolved in DMSO and then diluted with 0.9% sterile saline such that the concentration of DMSO did not exceed 1% of the injected solutions. For chemogenetic silencing (*R26*$^{ds\text{-}hM4di}$) and activation (*R26*$^{ds\text{-}hM3di}$)

experiments on protective reflexes, all mice received i.p. injections of CNO (2 mg/kg) on the first day, and of saline solution on the following one. For corrective responses, mice were treated on the first day with saline and on the following day with CNO. For chemogenetic silencing using PSEM^{89S} (R&D Systems), the drug was dissolved in 0.9% sterile saline and injected i.p. (30 mg/kg) on the second testing day, whereas saline solution was injected as control on the first day.

Behavioral Testing—6- to 8-week old mice of both sexes were used for behavioral testing upon ablation or chemogenetic manipulation of neuronal activity. For ablation experiments mice were tested 2 weeks after the first DTX injection. The same mouse underwent all the behavioral tests, except histamine-induced scratch. At the experimental end point spinal cord and brain tissues were collected for anatomical analysis and to verify the efficiency of the DTX-mediated cell loss. For CNO-induced silencing and activation 6- to 7-week old mice were tested 10 and 20 minutes following i.p. injection of the drug, respectively. CNO-injected mice were tested on selected behavioral paradigms, as we wanted to limit eventual side effects due to repeated drug administrations in the same animal. For PSEM^{89S}-induced silencing 8-week old mice were tested 30 minutes after being injected i.p. with the drug.

All tests were conducted during the same portion of circadian cycle, with sensory testing conducted in the morning and motor testing in the early afternoon. The experimenter was blind to the genotype of the animals.

von Frey Test: Animals were placed on an elevated wire grid for the two days prior to testing for 1 hour as acclimatization. On the experimental day mice were placed on the grid for 15 minutes for habituation, before their plantar paws were stimulated with calibrated von Frey monofilaments (0.016 – 4g). The paw withdrawal threshold was determined using an adapted up-down method (Bonin et al., 2014; Chaplan et al., 1994). The paw was stimulated with increasingly stronger force starting from the 0.016g filament, until a withdrawal response was observed. Once a successful event was obtained, the filament force was gradually decreased until cessation of the motor response. At this point, the force of the filament was newly increased until a new successful withdrawal event. The filament force that induced twice a withdrawal response was defined as threshold. The number of stimulations, delivered with at least 30 seconds interval and alternating the left and right paws, was not restricted to five as in Bonin et al. 2014, but never exceeded ten.

Non-noxious Mechanical Withdrawal (brush) Test: After the von Frey testing, mice were let to rest on the grid for 20 minutes and then stimulated with a paintbrush. The light stroking was applied in a heel to toe direction. The stimulation was repeated 10 times alternating left and right paws, with at least a minute interval. The percentage of withdrawal reflex responses elicited out of the total number of brush strokes applied was calculated.

Noxious Mechanical Withdrawal (pinprick) Test: After the brush testing, mice were let to rest on the grid for 20 minutes and then stimulated with an Austerlitz insect pin (Tip diameter 0.02 mm; Fine Science Tools). The pin was gently applied to the plantar surface of the paw, alternating between left and right hindpaws. The stimulation was repeated 10 times,

with at least 1 minute interval. The percentage of withdrawal reflex responses elicited out of the total number of pinprick stimulations was calculated.

Chloroquine- and histamine-induced scratching: After the withdrawal responses had been assessed, mice were acclimatized to the plexiglass chamber for 1 hr for the following two to three days. On the experimental day, 200 μg of chloroquine were injected subcutaneously in the nape of the neck using a 0.5 ml insulin syringe with a 29G1/2 needle (Exel). A separate cohort of mice was tested for their responses to histamine, by injecting 100 μg of histamine subcutaneously. Animals were video-recorded (Panasonic SDR-S26) for 30 minutes after injection. A single scratch bout was defined as every time the mouse hindlimb executed a full circular trajectory around the itchy spot. Videos were blindly scored by the experimenter and for each scratch episode, the time of occurrence, the duration and number of bouts were recorded. Raster plots were generated in R, using the ggplot package.

Narrow Beam Test: One week after the sensory tests were performed, animals were trained to cross an elevated 1 meter long, 25 mm wide beam. No differences in performance were observed during this training. In the following days, mice were tested on the elevated narrower beams (12 mm, 5 mm rectangular beams and 25 mm and 5 mm circular beams). Individual trials were video-recorded using two high speed cameras (mV Blue Cougar XD; 200 frame/second), capturing the performance from a lateral and a bottom view. Each mouse crossed three times each beam, and the total number of slips in the three runs was calculated by analyzing the videos frame by frame using the Simi Motion Analysis System.

Uneven Ladder Beam Test: One day after the narrow beam tests were performed, animals were tested onto the uneven ladder. Individual trials were video-recorded using two high speed cameras (mV Blue Cougar XD; 200 frame/second), capturing the performance from a lateral and a bottom view. Each mouse crossed three times the ladder, and the starting side was alternated at each trial. The total number of slips in the three runs was calculated by analyzing the videos frame by frame using the Simi Motion Analysis System.

Quantification and Statistical Analysis—All statistical analyses were done in Prism. We used two different statistical methods to compare multiple cohorts of mice: one-way ANOVA with Dunnett's post hoc test or two-way ANOVA with Bonferroni's post hoc test. The one-way ANOVA was used to statistically compare the results of each test (one variable) across genotypes and the two-way ANOVA to compare data with two variables, like stimulus and lamina or genotype and CNO or genotype and beam width. Our comparison indicates that controls across genotypes do not vary, but the ablated mice show a significant divergence from the control groups. We also did pairwise comparisons for each genotype and each experimental group using the two-tailed Student's t-test (paired or unpaired according to the experimental group) and obtained the same significant differences as presented in the one-way or two-way ANOVA analysis (**see** Table S1, for detailed pairwise Student's t-test comparison).

Supplementary Material

Refer to Web version on PubMed Central for supplementary material.

ACKNOWLEDGEMENTS

We thank Stephanie Koch and Sónia Paixão for discussion and comments on the manuscript. We thank Tomoko Velasquez for generating the Lmx1b antibody. This work was supported by NIH Grant NS080586, NS086372 and NS111643 to M.G., G.G. was supported by an EMBO postdoctoral fellowship (ALTF 13-2015), Salk Pioneer Scholar Award and Salk Women in Science Award. S.D.C. was supported by the Bert and Ethel Aginsky Research Scholar Award and the H.A. and Mary K. Chapman Charitable Trust. R.P.S. was supported by NIH Grant NS107364, and P.H. by David Scaife Foundation.

REFERENCES

Abraira VE, and Ginty DD (2013). The Sensory Neurons of Touch. Neuron 79, 618–639. [PubMed: 23972592]

Abraira VE, Kuehn ED, Chirila AM, Springel MW, Toliver AA, Zimmerman AL, Orefice LL, Boyle KA, Bai L, Song BJ, et al. (2017). The Cellular and Synaptic Architecture of the Mechanosensory Dorsal Horn. Cell 168, 295–310.e19. [PubMed: 28041852]

Akiyama T, Merrill AW, Zanotto K, Carstens MI, and Carstens E (2009). Scratching behavior and Fos expression in superficial dorsal horn elicited by protease-activated receptor agonists and other itch mediators in mice. J. Pharmacol. Exp. Ther. 329, 945–951. [PubMed: 19293390]

Albisetti GW, Pagani M, Platonova E, Hösli L, Johannssen HC, Fritschy J-M, Wildner H, and Zeilhofer HU (2019). Dorsal Horn Gastrin-Releasing Peptide Expressing Neurons Transmit Spinal Itch But Not Pain Signals. J. Neurosci. 39, 2238–2250. [PubMed: 30655357]

Arcourt A, Gorham L, Dhandapani R, Prato V, Taberner FJ, Wende H, Gangadharan V, Birchmeier C, Heppenstall PA, and Lechner SG (2017). Touch Receptor-Derived Sensory Information Alleviates Acute Pain Signaling and Fine-Tunes Nociceptive Reflex Coordination. Neuron 93, 179–193. [PubMed: 27989460]

Del Barrio MG, Bourane S, Grossmann K, Schule R, Britsch S, O'Leary DD, and Goulding M (2013). A transcription factor code defines nine sensory interneuron subtypes in the mechanosensory area of the spinal cord. PLoS One 8, e77928. [PubMed: 24223744]

Basbaum AI, Bautista DM, Scherrer G, and Julius D (2009). Cellular and molecular mechanisms of pain. Cell 139, 267–284. [PubMed: 19837031]

Bell AM, Gutierrez-Mecinas M, Polgár E, and Todd AJ (2016). Spinal neurons that contain gastrin-releasing peptide seldom express Fos or phosphorylate extracellular signal-regulated kinases in response to intradermal chloroquine. Mol. Pain 12.

Bonin RP, Bories C, and De Koninck Y (2014). A simplified up-down method (SUDO) for measuring mechanical nociception in rodents using von Frey filaments. Mol. Pain 10, 26. [PubMed: 24739328]

Bourane S, Grossmann KS, Britz O, Dalet A, Del Barrio MG, Stam FJ, Garcia-Campmany L, Koch S, and Goulding M (2015a). Identification of a spinal circuit for light touch and fine motor control. Cell 160, 503–515. [PubMed: 25635458]

Bourane S, Duan B, Koch SC, Dalet A, Britz O, Garcia-Campmany L, Kim E, Cheng L, Ghosh A, Ma Q, et al. (2015b). Gate control of mechanical itch by a subpopulation of spinal cord interneurons. Science 350, 550–554. [PubMed: 26516282]

Braz J, Solorzano C, Wang X, and Basbaum AI (2014). Transmitting pain and itch messages: a contemporary view of the spinal cord circuits that generate gate control. Neuron 82, 522–536. [PubMed: 24811377]

Britz O, Zhang J, Grossmann KS, Dyck J, Kim JC, Dymecki S, Gosgnach S, and Goulding M (2015). A genetically defined asymmetry underlies the inhibitory control of flexor-extensor locomotor movements. Elife 4.

Chaplan SR, Bach FW, Pogrel JW, Chung JM, and Yaksh TL (1994). Quantitative assessment of tactile allodynia in the rat paw. J. Neurosci. Methods 53, 55–63. [PubMed: 7990513]

Chen S, Yang G, Zhu Y, Liu Z, Wang W, Wei J, Li K, Wu J, Chen Z, Li Y, et al. (2016). A Comparative Study of Three Interneuron Types in the Rat Spinal Cord. PLoS One 11, e0162969. [PubMed: 27658248]

Cheng L, Duan B, Huang T, Zhang Y, Chen Y, Britz O, Garcia-Campmany L, Ren X, Vong L, Lowell BB, et al. (2017). Identification of spinal circuits involved in touch-evoked dynamic mechanical pain. Nat. Neurosci. 20, 804–814. [PubMed: 28436981]

Chou SJ, Babot Z, Leingartner A, Studer M, Nakagawa Y, and O'Leary DDM (2013). Geniculocortical input drives genetic distinctions between primary and higher-order visual areas. Science 340, 1239–1242. [PubMed: 23744949]

Christensen AJ, Iyer SM, François A, Vyas S, Ramakrishnan C, Vesuna S, Deisseroth K, Scherrer G, and Delp SL (2016). In Vivo Interrogation of Spinal Mechanosensory Circuits. Cell Rep. 17, 1699–1710. [PubMed: 27806306]

Craig A.D. (Bud) (2003). Pain mechanisms: Labeled Lines Versus Convergence in Central Processing. Annu. Rev. Neurosci. 26, 1–30. [PubMed: 12651967]

Crone SA, Quinlan KA, Zagoraiou L, Droho S, Restrepo CE, Lundfald L, Endo T, Setlak J, Jessell TM, Kiehn O, et al. (2008). Genetic ablation of V2a ipsilateral interneurons disrupts left-right locomotor coordination in mammalian spinal cord. Neuron 60, 70–83. [PubMed: 18940589]

Delmas P, Hao J, and Rodat-Despoix L (2011). Molecular mechanisms of mechanotransduction in mammalian sensory neurons. Nat. Rev. Neurosci. 12, 139–153. [PubMed: 21304548]

Doetsch GS (2002). Patterns in the brain: Neuronal population coding in the somatosensory system. Physiol. Behav. 69, 187–201.

Dong X, and Dong X (2018). Peripheral and Central Mechanisms of Itch. Neuron 98, 482–494. [PubMed: 29723501]

Duan B, Cheng L, Bourane S, Britz O, Padilla C, Garcia-campmany L, Krashes M, Knowlton W, Velasquez T, Ren X, et al. (2014). Identification of Spinal Circuits Transmitting and Gating Mechanical Pain. Cell 159, 1417–1432. [PubMed: 25467445]

Fatima M, Ren X, Pan H, Slade H, Asmar AJ, Xiong C, Shi A, Xiong E, Wang L, and Duan B (2019). Spinal somatostatin-positive interneurons transmit chemical itch. Pain 1. [PubMed: 30086114]

Forssberg H (1979). Stumbling corrective reaction: a phase-dependent compensatory reaction during locomotion. J. Neurophysiol. 42, 936–953. [PubMed: 479924]

Gatto G, Smith KM, Ross SE, and Goulding M (2019). Neuronal diversity in the somatosensory system: bridging the gap between cell type and function. Curr. Opin. Neurobiol. 56, 167–174. [PubMed: 30953870]

Gutierrez-Mecinas M, Furuta T, Watanabe M, and Todd AJ (2016). A quantitative study of neurochemically defined excitatory interneuron populations in laminae I-III of the mouse spinal cord. Mol. Pain 12, 174480691662906.

Gutierrez-Mecinas M, Bell AM, Marin A, Taylor R, Boyle KA, Furuta T, Watanabe M, Polgár E, and Todd AJ (2017). Preprotachykinin A is expressed by a distinct population of excitatory neurons in the mouse superficial spinal dorsal horn including cells that respond to noxious and pruritic stimuli. Pain 158, 440–456. [PubMed: 27902570]

Gutierrez-Mecinas M, Bell AM, Shepherd F, Polgár E, Watanabe M, Furuta T, and Todd AJ (2019). Expression of cholecystokinin by neurons in mouse spinal dorsal horn. J. Comp. Neurol. 527, 1857–1871. [PubMed: 30734936]

Han L, and Dong X (2014). Itch mechanisms and circuits. Annu. Rev. Biophys. 43, 331–355. [PubMed: 24819620]

Han L, Ma C, Liu Q, Weng H-J, Cui Y, Tang Z, Kim Y, Nie H, Qu L, Patel KN, et al. (2013). A subpopulation of nociceptors specifically linked to itch. Nat. Neurosci. 16, 174–182. [PubMed: 23263443]

Handwerker HO (2014). Itch Hypotheses: From Pattern to Specificity and to Population Coding (CRC Press/Taylor & Francis(c) 2014 by Taylor & Francis Group, LLC.).

Häring M, Zeisel A, Hochgerner H, Rinwa P, Jakobsson JET, Lönnerberg P, La Manno G, Sharma N, Borgius L, Kiehn O, et al. (2018). Neuronal atlas of the dorsal horn defines its architecture and links sensory input to transcriptional cell types. Nat. Neurosci. 21, 869–880. [PubMed: 29686262]

He M, Tucciarone J, Lee SH, Nigro MJ, Kim Y, Levine JM, Kelly SM, Krugikov I, Wu P, Chen Y, et al. (2016). Strategies and Tools for Combinatorial Targeting of GABAergic Neurons in Mouse Cerebral Cortex. Neuron 91, 1228–1243. [PubMed: 27618674]

Holstege JC, de Graaff W, Hossaini M, Cardona Cano S, Jaarsma D, van den Akker E, and Deschamps J (2008). Loss of Hoxb8 alters spinal dorsal laminae and sensory responses in mice. Proc. Natl. Acad. Sci. U. S. A. 105, 6338–6343. [PubMed: 18430798]

Hu J, Huang T, Li T, Guo Z, and Cheng L (2012). c-Maf Is Required for the Development of Dorsal Horn Laminae III/IV Neurons and Mechanoreceptive DRG Axon Projections. J. Neurosci. 32, 5362–5373. [PubMed: 22514301]

Huang J, Polgár E, Solinski HJ, Mishra SK, Tseng P-Y, Iwagaki N, Boyle KA, Dickie AC, Kriegbaum MC, Wildner H, et al. (2018). Circuit dissection of the role of somatostatin in itch and pain. Nat. Neurosci. 21, 707–716. [PubMed: 29556030]

Huang T, Lin S-H, Malewicz NM, Zhang Y, Zhang Y, Goulding M, LaMotte RH, and Ma Q (2019). Identifying the pathways required for coping behaviours associated with sustained pain. Nature 565, 86–90. [PubMed: 30532001]

Jenkins BA, and Lumpkin EA (2017). Developing a sense of touch. Development 144, 4078–4090. [PubMed: 29138290]

Jensen RT, Battey JF, Spindel ER, and Benya RV (2008). International union of pharmacology. LXVIII. Mammalian bombesin receptors: Nomenclature, distribution, pharmacology, signaling, and functions in normal and disease states. Pharmacol. Rev. 60, 1–42. [PubMed: 18055507]

Kania A, Johnson RL, and Jessell TM (2000). Coordinate roles for LIM homeobox genes in directing the dorsoventral trajectory of motor axons in the vertebrate limb. Cell 102, 161–173. [PubMed: 10943837]

Koch SC, Del Barrio MG, Dalet A, Gatto G, Günther T, Zhang J, Seidler B, Saur D, Schüle R, and Goulding M (2017). RORβ Spinal Interneurons Gate Sensory Transmission during Locomotion to Secure a Fluid Walking Gait. Neuron 96, 1419–1431.e5. [PubMed: 29224725]

Leinninger GM, Opland DM, Jo YH, Faouzi M, Christensen L, Cappellucci LA, Rhodes CJ, Gnegy ME, Becker JB, Pothos EN, et al. (2011). Leptin action via neurotensin neurons controls orexin, the mesolimbic dopamine system and energy balance. Cell Metab. 14, 313–323. [PubMed: 21907138]

Levine AJ, Hinckley CA, Hilde KL, Driscoll SP, Poon TH, Montgomery JM, and Pfaff SL (2014). Identification of a cellular node for motor control pathways. Nat Neurosci 17, 586–593. [PubMed: 24609464]

Liu Y, Latremoliere A, Li X, Zhang Z, Chen M, Wang X, Fang C, Zhu J, Alexandre C, Gao Z, et al. (2018). Touch and tactile neuropathic pain sensitivity are set by corticospinal projections. Nature 561, 547–550. [PubMed: 30209395]

Ma Q (2010). Labeled lines meet and talk: Population coding of somatic sensations. J. Clin. Invest. 120, 3773–3778. [PubMed: 21041959]

Madisen L, Zwingman TA, Sunkin SM, Oh SW, Zariwala HA, Gu H, Ng LL, Palmiter RD, Hawrylycz MJ, Jones AR, et al. (2010). A robust and high-throughput Cre reporting and characterization system for the whole mouse brain. Nat. Neurosci. 13, 133–140. [PubMed: 20023653]

Madisen L, Garner AR, Shimaoka D, Chuong AS, Klapoetke NC, Li L, van der Bourg A, Niino Y, Egolf L, Monetti C, et al. (2015). Transgenic mice for intersectional targeting of neural sensors and effectors with high specificity and performance. Neuron 85, 942–958. [PubMed: 25741722]

Mar L, Yang FC, and Ma Q (2012). Genetic marking and characterization of Tac2-expressing neurons in the central and peripheral nervous system. Mol. Brain 5, 3. [PubMed: 22272772]

McCoy ES, Taylor-Blake B, Street SE, Pribisko AL, Zheng J, and Zylka MJ (2013). Peptidergic CGRPα primary sensory neurons encode heat and itch and tonically suppress sensitivity to cold. Neuron 78, 138–151. [PubMed: 23523592]

McGlone F, and Reilly D (2010). The cutaneous sensory system. Neurosci. Biobehav. Rev. 34, 148–159. [PubMed: 19712693]

Melzack R, and Wall PD (1965). Pain mechanisms: a new theory. Science 150, 971–979. [PubMed: 5320816]

Mishra SK, and Hoon M a (2013). The cells and circuitry for itch responses in mice. Science 340, 968–971. [PubMed: 23704570]

Moehring F, Halder P, Seal RP, and Stucky CL (2018). Uncovering the Cells and Circuits of Touch in Normal and Pathological Settings. Neuron 100, 349–360. [PubMed: 30359601]

Müller J (1837). Handbuch der Physiologie des Menschen. (von Hoelscher Coblenz verlag, Coblenz J).

Norrsell U, Finger S, and Lajonchere C (1999). Cutaneous sensory spots and the “law of specific nerve energies”: history and development of ideas. Brain Res. Bull. 48, 457–465. [PubMed: 10372506]

Orefice LL, Zimmerman AL, Chirila AM, Sleboda SJ, Head JP, Ginty Correspondence DD, and Ginty DD (2016). Peripheral Mechanosensory Neuron Dysfunction Underlies Tactile and Behavioral Deficits in Mouse Models of ASDs. Cell 166, 299–313. [PubMed: 27293187]

Paixão S, Loschek L, Gaitanos L, Alcalà Morales P, Goulding M, and Klein R (2019). Identification of Spinal Neurons Contributing to the Dorsal Column Projection Mediating Fine Touch and Corrective Motor Movements. Neuron 104, 749–764.e6. [PubMed: 31586516]

Peirs C, Williams SPG, Zhao X, Walsh CE, Gedeon JY, Cagle NE, Goldring AC, Hioki H, Liu Z, Marell PS, et al. (2015). Dorsal Horn Circuits for Persistent Mechanical Pain. Neuron 87, 797–812. [PubMed: 26291162]

Peirs C, Williams SPG, Zhao X, Arokiaraj CM, Ferreira DW, Noh M, Smith KM, Halder P, Corrigan KA, Gedeon JY et al. (202X)

Petitjean H, B. Bourojeni F, Tsao D, Davidova A, Sotocinal SG, Mogil JS, Kania A, and Sharif-Naeini R. (2019). Recruitment of Spinoparabrachial Neurons by Dorsal Horn Calretinin Neurons. Cell Rep. 28, 1429–1438.e4. [PubMed: 31390558]

Polgár E, Fowler JH, McGill MM, and Todd AJ (1999). The types of neuron which contain protein kinase C gamma in rat spinal cord. Brain Res. 833, 71–80. [PubMed: 10375678]

Rossignol S, Dubuc R, and Gossard J-P (2006). Dynamic Sensorimotor Interactions in Locomotion. Physiol. Rev. 86, 594–603.

Rottkamp CA, Lobur KJ, Wladyka CL, Lucky AK, and O’Gorman S (2008). Pbx3 is required for normal locomotion and dorsal horn development. Dev. Biol. 314, 23–39. [PubMed: 18155191]

Sathyamurthy A, Johnson KR, Matson KJE, Dobrott CI, Li L, Ryba AR, Bergman TB, Kelly MC, Kelley MW, and Levine AJ (2018). Massively Parallel Single Nucleus Transcriptional Profiling Defines Spinal Cord Neurons and Their Activity during Behavior. Cell Rep. 22, 2216–2225. [PubMed: 29466745]

Schouenborg J, Weng HR, Kalliomäki J, and Holmberg H (1995). A survey of spinal dorsal horn neurones encoding the spatial organization of withdrawal reflexes in the rat. Exp. Brain Res. 106, 19–27. [PubMed: 8542974]

Sciolino NR, Plummer NW, Chen YW, Alexander GM, Robertson SD, Dudek SM, McElligott ZA, and Jensen P (2016). Recombinase-Dependent Mouse Lines for Chemogenetic Activation of Genetically Defined Cell Types. Cell Rep. 15, 2563–2573. [PubMed: 27264177]

Smith KM, Browne TJ, Davis OC, Coyle A, Boyle KA, Watanabe M, Dickinson SA, Iredale JA, Gradwell MA, Jobling P, et al. (2019). Calretinin positive neurons form an excitatory amplifier network in the spinal cord dorsal horn. Elife 8.

Stam FJ, Hendricks TJ, Zhang J, Geiman EJ, Francius C, Labosky PA, Clotman F, and Goulding M (2012). Renshaw cell interneuron specialization is controlled by a temporally restricted transcription factor program. Development 139, 179–190. [PubMed: 22115757]

Sun Y-G, and Chen Z-F (2007). A gastrin-releasing peptide receptor mediates the itch sensation in the spinal cord. Nature 448, 700–703. [PubMed: 17653196]

Sun YG, Zhao ZQ, Meng XL, Yin J, Liu XY, and Chen ZF (2009). Cellular basis of itch sensation. Science 325, 1531–1534. [PubMed: 19661382]

Szabo NE, da Silva RV, Sotocinal SG, Zeilhofer HU, Mogil JS, and Kania A (2015). Hoxb8 Intersection Defines a Role for Lmx1b in Excitatory Dorsal Horn Neuron Development, Spinofugal Connectivity, and Nociception. J. Neurosci. 35, 5233–5246. [PubMed: 25834049]

Taniguchi H, He M, Wu P, Kim S, Paik R, Sugino K, Kvitsani D, Fu Y, Lu J, Lin Y, et al. (2011). A Resource of Cre Driver Lines for Genetic Targeting of GABAergic Neurons in Cerebral Cortex. Neuron 71, 995–1013. [PubMed: 21943598]

Todd AJ (2010). Neuronal circuitry for pain processing in the dorsal horn. Nat. Rev. Neurosci. 11, 823–836. [PubMed: 21068766]

Usoskin D, Furlan A, Islam S, Abdo H, Lönnerberg P, Lou D, Hjerling-Leffler J, Haeggström J, Kharchenko O, Kharchenko PV, et al. (2015). Unbiased classification of sensory neuron types by large-scale single-cell RNA sequencing. Nat. Neurosci. 18, 145–153. [PubMed: 25420068]

Villeda SA, Akopians AL, Babayan AH, Basbaum AI, and Phelps PE (2006). Absence of Reelin results in altered nociception and aberrant neuronal positioning in the dorsal spinal cord. Neuroscience 139, 1385–1396. [PubMed: 16580148]

Wang X, Zhang J, Eberhart D, Urban R, Meda K, Solorzano C, Yamanaka H, Rice D, and Basbaum AII (2013). Excitatory superficial dorsal horn interneurons are functionally heterogeneous and required for the full behavioral expression of pain and itch. Neuron 78, 312–324. [PubMed: 23622066]

Wende H, Lechner SG, Cheret C, Bourane S, Kolanczyk ME, Pattyn A, Reuter K, Munier FL, Carroll P, Lewin GR, et al. (2012). The transcription factor c-Maf controls touch receptor development and function. Science 335, 1373–1376. [PubMed: 22345400]

Xu Y, Lopes C, Wende H, Guo Z, Cheng L, Birchmeier C, and Ma Q (2013). Ontogeny of excitatory spinal neurons processing distinct somatic sensory modalities. J. Neurosci. 33, 14738–14748. [PubMed: 24027274]

Zeisel A, Hochgerner H, Lönnerberg P, Johnsson A, Memic F, van der Zwan J, Häring M, Braun E, Borm LE, La Manno G, et al. (2018). Molecular Architecture of the Mouse Nervous System. Cell 174, 999–1014.e22. [PubMed: 30096314]

Zhao Z-Q, Wan L, Liu X-Y, Huo F-Q, Li H, Barry DM, Krieger S, Kim S, Liu Z-C, Xu J, et al. (2014). Cross-Inhibition of NMBR and GRPR Signaling Maintains Normal Histaminergic Itch Transmission. J. Neurosci. 34, 12402–12414. [PubMed: 25209280]

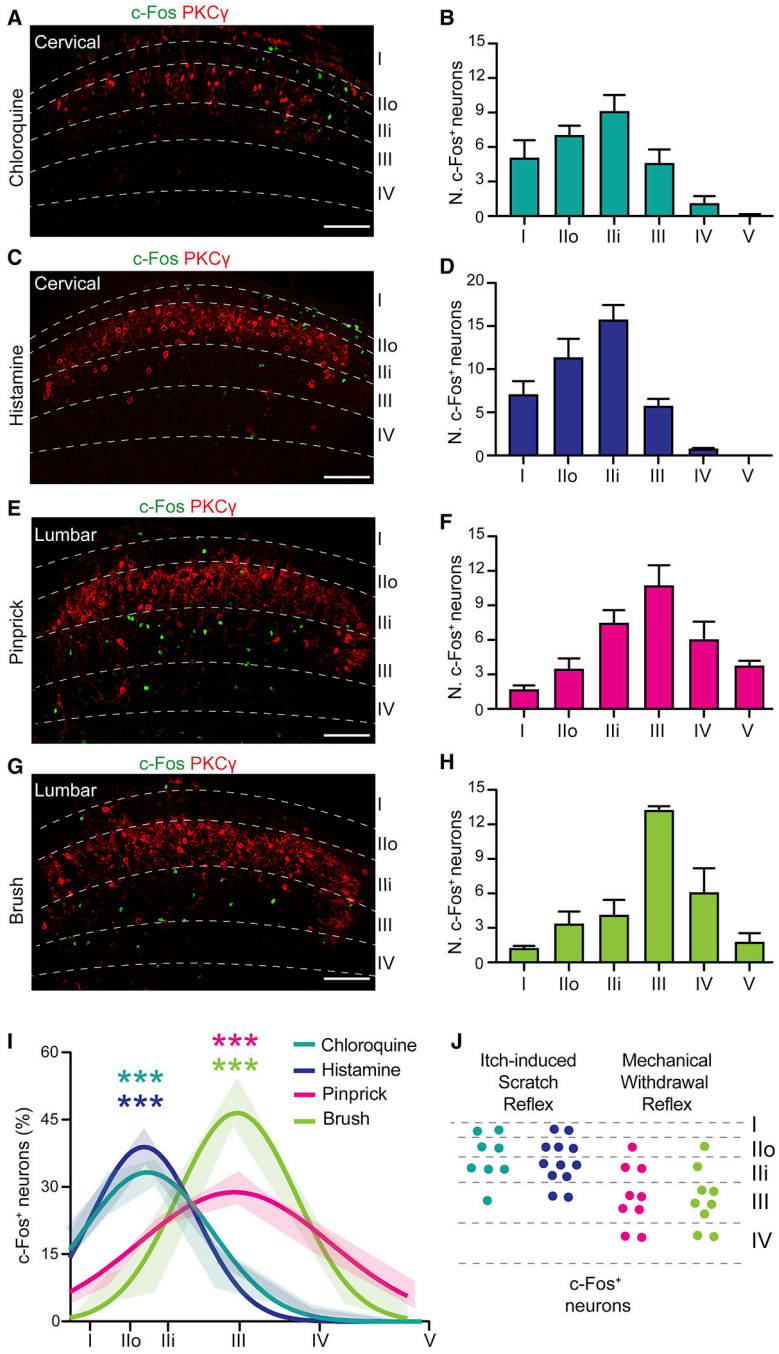

Figure 1. Sensory-modality specific neuronal activation peaks in distinct laminar patterns

(A,C,E,G) 30 μm sections through the cervical (A,C) or lumbar (E,G) cord of P56 mice stained with antibodies to c-Fos (green) and PKCγ (red) after subcutaneous injection of chloroquine (A) and histamine (C) into the nape of the neck, and after pinprick (E) or light brush (G) stimulation of the ipsilateral hindpaw. Scale bar 100 μm.

(B,D,F,H) Absolute number of c-Fos$^+$ neurons (30 μm hemisection) present in each lamina after stimulation with chloroquine (B), histamine (D), pinprick (F) or light brush (H). Data

are presented as mean ± SEM. N= 3 mice for pruritogens and brush, and N=4 mice for pinprick.

(G) Non-linear fit distributions of the percentage of c-Fos$^+$ neurons present across the different spinal laminae of mice stimulated with chloroquine (cyan), histamine (cobalt blue), pinprick (magenta) or brush (green). Shaded areas represent the SEM of each distribution. The four curve fits were compared. Significance of pruritogens vs pinprick and brush is shown with magenta and green asterisks, respectively. Brush and pinprick responses were not significantly different.

(H) Schematic showing the distributions of c-Fos$^+$ neurons across the distinct spinal laminae. Each dot represents 3 neurons. **See also** Figure S1 **and** Table S1.

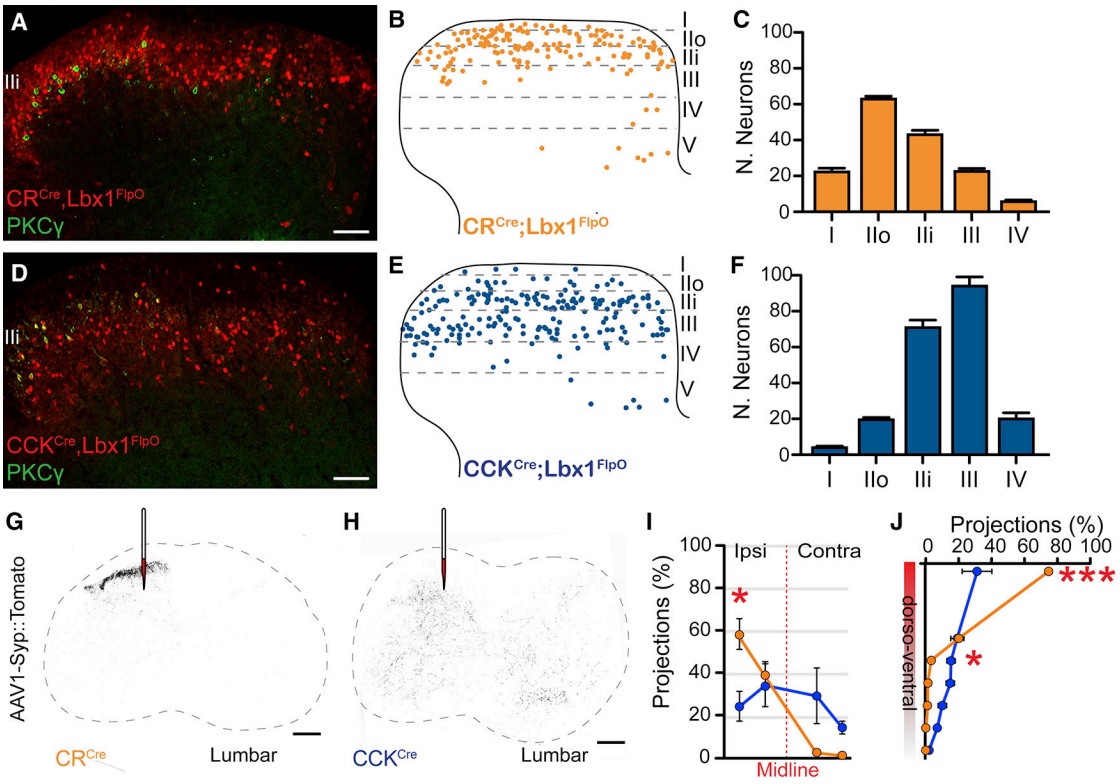

Figure 2. Spatial distribution and molecular identity define distinct spinal circuits

(A,D) 40 μm transverse sections through the lumbar dorsal spinal cord of *CR^{Cre};Lbx1^{FlpO};R26$^{ds\text{-}Tom}$* (A) and *CCK^{Cre};Lbx1^{FlpO};R26$^{ds\text{-}Tom}$* (D) mice. Each section was stained with antibodies to Td-Tomato (red) and PKCγ (green). Scale bar 100 μm.

(B,E) Schematic illustrating the average distribution across the lumbar dorsal spinal laminae of INs targeted using *CR^{Cre};Lbx1^{FlpO}* (B) and *CCK^{Cre};Lbx1^{FlpO}* (E) lineage tracings.

(C,F) Absolute numbers of CR^{Cre};Lbx1^{FlpO} INs (C) and CCK^{Cre};Lbx1^{FlpO} INs (F) per 40 μm hemisection of the lumbar spinal cord. N=10 mice for *CR^{Cre};Lbx1^{FlpO}* and 3 for *CCK^{Cre};Lbx1^{FlpO}*.

(I,J) 30 μm transverse sections through the lumbar dorsal spinal cord of *CR^{Cre}* (I) and *CCK^{Cre}* (J) mice injected unilaterally at L3-L5 with AAV1-Syp::Tomato. Each section was stained with antibodies to Td-Tomato. Scale bar 100 μm.

(K,L) Percentages of ipsilateral/contralateral (K) and dorso/ventral (L) synaptic puncta compared to total projections of CR^{Cre} INs (K) and CCK^{Cre} INs (L) per 30 μm hemisection of the lumbar spinal cord. N=3 mice per genotype. Statistical analysis was done using two-way ANOVA, followed by Bonferroni's post hoc test, with *p<0.05 and ***p<0.001.

(G, H) 30-μm transverse sections through the lumbar dorsal spinal cord of CRCre (I) and CCKCre (J) mice injected unilaterally at L3–L5 with AAV1-Syp::Tomato. Each section was stained with antibodies to Td-Tomato. Scale bar: 100 μm Both instances of Cre are superscript. CR^{Cre} CCK^{Cre}

Data are presented as mean ± SEM. **See also** Figure S2 **and** Table S1.

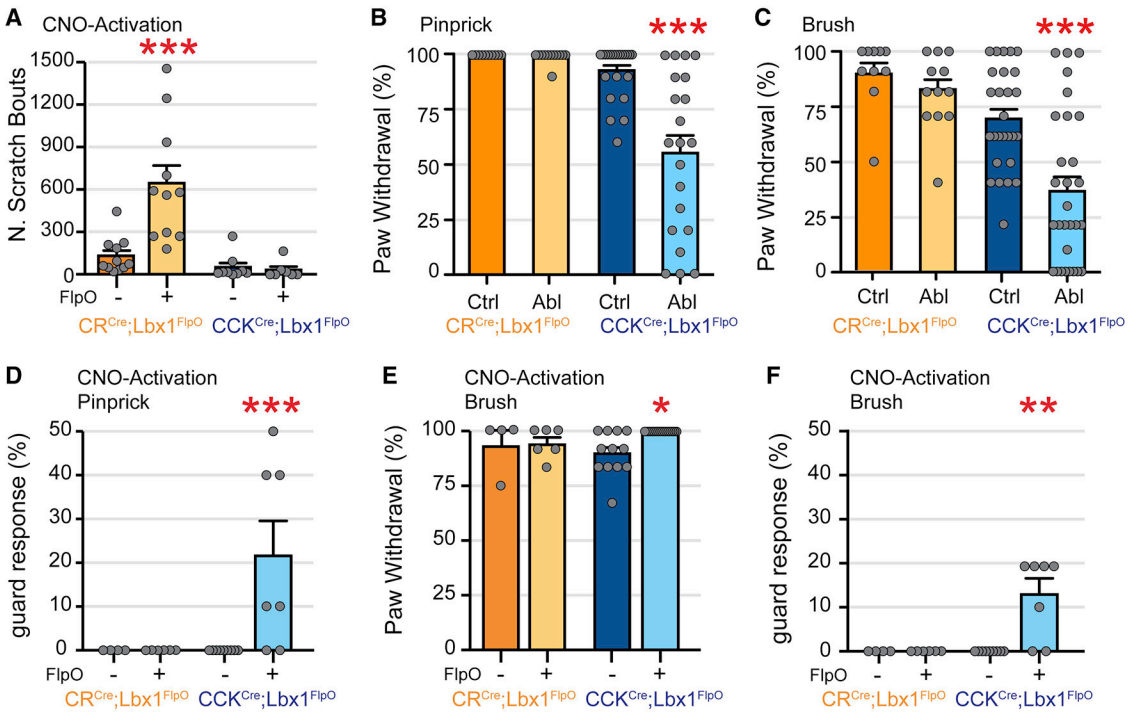

Figure 3. Scratch and withdrawal reflexes are driven by distinct spatially confined excitatory networks.

(A) CNO-induced neuronal activation in CR^{Cre};$Lbx1^{FlpO}$ INs, but not in CCK^{Cre};$Lbx1^{FlpO}$ INs, elicits a spontaneous scratch response. Darker bar colors indicate the control mice lacking the *Lbx1^{FlpO}* allele.

(B,C) Decreased paw sensitivity to noxious (B) and non-noxious (C) mechanical stimuli in mice upon ablation (Abl) of CCK^{Cre};$Lbx1^{FlpO}$ INs but not CR^{Cre};$Lbx1^{FlpO}$ INs. Controls (Ctrl) are either *CR^{Cre}; Lbx1^{FlpO}* mice treated with saline or *CCK^{Cre} and FlpO*-negative mice treated with DTX.

(D,F) Increased frequency of paw held in guard position upon noxious (D) and non-noxious (F) mechanical stimulation of the footpad after CNO-induced activation of CCK^{Cre};$Lbx1^{FlpO}$ INs but not CR^{Cre};$Lbx1^{FlpO}$ INs. Controls are *FlpO*-negative mice treated with CNO.

(E) Increased percentage of withdrawal response to non-noxious mechanical stimulus observed upon CNO-driven neuron activation in *CCK^{Cre};Lbx1^{FlpO}* but not in *CR^{Cre};Lbx1^{FlpO}* mice. Controls are *FlpO*-negative mice treated with CNO.

Data are presented as mean ± SEM. Statistical analysis was done using one-way ANOVA followed by Dunnett's post hoc test with all genotypes compared to *CR^{Cre};Lbx1^{FlpO-}* (A) or *CR^{Cre};Lbx1^{FlpO+}* saline-treated (C,D,F) or *CCK^{Cre};Lbx1^{FlpO-}* (E) mice, with *p<0.05, ***p<0.001. Each mouse analyzed is represented with a grey filled circle. **See also** Figure S3, Videos S1–S5 **and** Table S1.

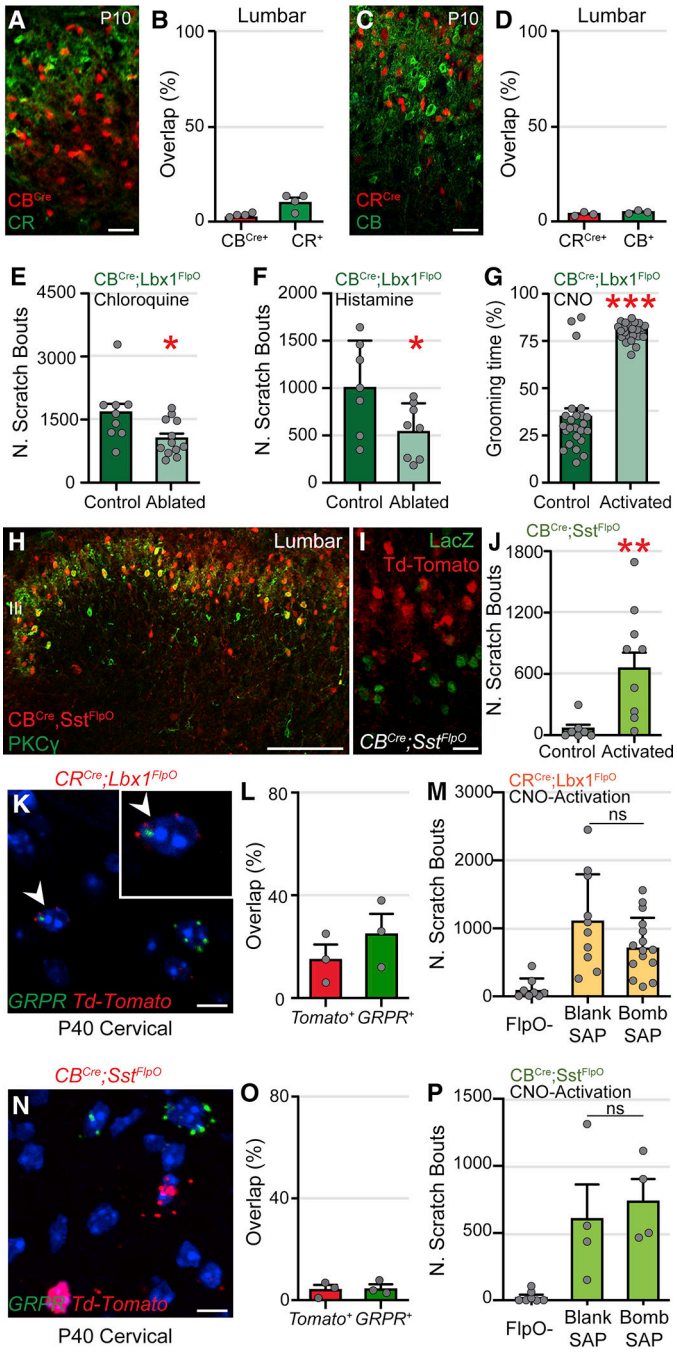

Figure 4. Population coding theory accounts for the chemical itch-induced scratch reflex

(A,C) 20 μm transverse sections through the P10 $CB^{Cre};R26^{Ai14\text{-}Tom}$ (A) and $CR^{Cre};Lbx1^{FlpO};R26^{ds\text{-}Tom}$ (C) lumbar dorsal spinal cords stained with antibodies to RFP (red) and CR (A) or CB (C) (green). Scale bar 40 μm.

(B,D) Graphs showing the percentage of neurons co-expressing *Cre* and CR (B) or CB (D) compared to the total number of Cre^+ INs or the total CR^+ (B) or CB^+ INs (D).

(E,F) CB^{Cre};$Lbx1^{FlpO}$ IN-ablated mice show a significant decrease in the scratch response to subcutaneous chloroquine (E) and histamine (F) injection compared to littermate controls. Controls are *Cre*$^{+}$ and *FlpO*$^{+}$ mice treated with saline instead of DTX.

(G) CNO-induced neuronal activation in $CB^{Cre};Lbx1^{FlpO}$ mice elicits a strong grooming behavior. Controls are *FlpO*-negative mice treated with CNO.

(H) 40 μm transverse sections through P56 $CB^{Cre};Sst^{FlpO};R26^{ds\text{-}Tom}$ lumbar dorsal spinal cord stained with antibodies to Td-Tomato (red) and PKCγ (green). Scale bar 100 μm.

(I) 20 μm transverse sections through the P10 $CB^{Cre};Sst^{FlpO};Tau^{ds\text{-}DTR};R26^{ds\text{-}Tom}$ lumbar dorsal spinal cords stained with antibodies to Td-Tomato (red) and LacZ (green). Scale bar 40 μm.

(J) Increased scratch response observed after CNO-activation in $CB^{Cre};Sst^{FlpO}$ mice compared to *FlpO*-negative littermate controls.

(K,N) 14 μm transverse sections through the P40 $CR^{Cre};Lbx1^{FlpO};R26^{ds\text{-}Tom}$ (K) and $CB^{Cre};Sst^{FlpO};R26^{ds\text{-}Tom}$ (N) cervical dorsal spinal cords stained with RNAscope probes to *Td-Tomato* (red) and *GRPR* (green) mRNA. Scale bar 10 μm.

(L,O) Graphs showing the percentage of neurons co-expressing $CR^{Cre};Lbx1^{FlpO};R26^{ds\text{-}Tom}$ (L) or $CB^{Cre};Sst^{FlpO};R26^{ds\text{-}Tom}$ (O) and *GRPR* compared to the total number of intersectionally labeled INs (red bar) or the total number of $GRPR^{+}$ INs (green bar).

(M,P) No changes in the spontaneous scratch behavior elicited upon CNO-driven activation of CR^{Cre};$Lbx1^{FlpO}$ INs (M) and CB^{Cre};Sst^{FlpO} INs (P) following ablation of $GRPR^{+}$ INs (Bomb-Sap) compared to controls (Blank-Sap). Note the increase in scratching in both conditions compared to *FlpO*-negative littermate controls. Statistical analysis was done using one-way ANOVA, followed by Dunnett's post hoc test with all genotypes compared to Blank-Sap treatment.

Data are presented as mean ± SEM. Statistical analysis was done using two-tailed Student's t-test with *p<0.05, **p<0.01 and ***p<0.001, unless otherwise stated. Each mouse analyzed is represented with a grey filled circle. **See also** Figure S4 **and** Table S1.

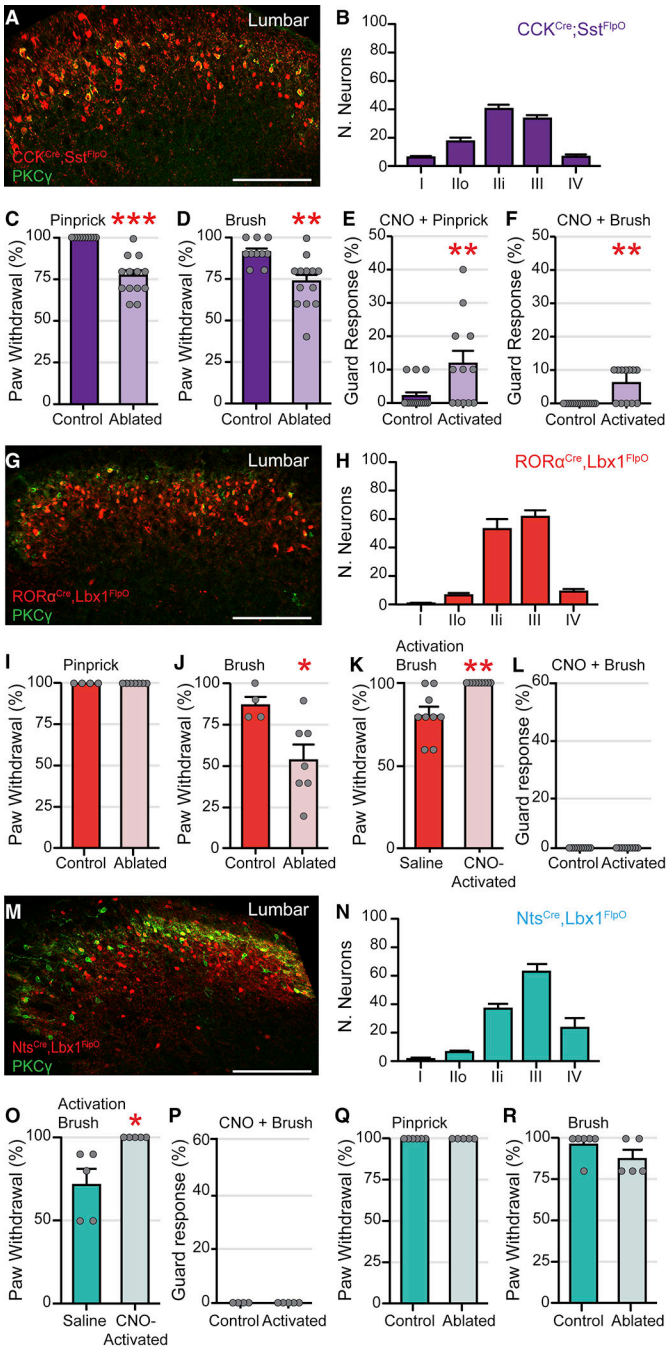

Figure 5. Distinct subsets of excitatory INs in laminae II/III cooperate to elicit the withdrawal reflex

(A,G,M) 40 μm transverse sections through P56 *CCK^{Cre};Sst^{FlpO};R26$^{ds\text{-}Tom}$* (A), *RORα^{Cre};Lbx1^{FlpO};R26$^{ds\text{-}Tom}$* (G) and *Nts^{Cre};Lbx1^{FlpO};R26$^{ds\text{-}Tom}$* (M) lumbar dorsal spinal cord stained with antibodies to Td-Tomato (red) and PKCγ (green). Scale bar 100 μm. (B,H,N) Absolute numbers of CCK^{Cre};Sst^{FlpO} INs (B), RORα^{Cre};Lbx1^{FlpO} INs (H) and Nts^{Cre};Lbx1^{FlpO} INs (N) per 40 μm hemisection of the lumbar spinal cord. N=6 mice for *CCK^{Cre};Sst^{FlpO}*, N=4 for *RORα^{Cre};Lbx1^{FlpO}* and N=3 for *Nts^{Cre};Lbx1^{FlpO}*.

(C,I,Q) Decreased paw sensitivity to noxious pinprick upon ablation of $CCK^{Cre};Sst^{FlpO}$ INs but no changes following the loss of $ROR\alpha^{Cre};Lbx1^{FlpO}$ (I) and $Nts^{Cre};Lbx1^{FlpO}$ INs (Q). Controls are Cre^{+} and $FlpO^{+}$ mice treated with saline instead of DTX.

(D,J,R) Decreased paw sensitivity to non-noxious brush upon ablation of $CCK^{Cre};Sst^{Flp}$ (C), $ROR\alpha^{Cre};Lbx1^{FlpO}$ INs but no significant changes upon the loss of $Nts^{Cre};Lbx1^{FlpO}$ INs (R). Controls are Cre^{+} and $FlpO^{+}$ mice treated with saline instead of DTX.

(E,F) Increased frequency of paw held in guard position upon noxious (E) and non-noxious (F) mechanical stimulation of the footpad after CNO-activation of $CCK^{Cre};Sst^{FlpO}$ INs, as opposed to similarly treated *FlpO*-negative controls.

(K,O) Increased percentage of withdrawal response to non-noxious mechanical stimulus observed upon CNO-driven neuron activation in $ROR\alpha^{Cre};hCdx2::FlpO$ (K) and $Nts^{Cre};Lbx1^{FlpO}$ (O) mice compared to *FlpO*-negative controls.

(L,P) Absence of paw held in guard position upon non-noxious mechanical stimulation of the footpad after CNO-induced activation of $ROR\alpha^{Cre};Lbx1^{FlpO}$ INs (L) and $Nts^{Cre};Lbx1^{FlpO}$ INs (P), and in similarly treated *FlpO*-negative controls.

Data are presented as mean ± SEM. Each mouse analyzed is represented with a grey filled circle. Statistical analysis was done using two-tailed Student's t-test with *p<0.1, **p<0.01 and ***p<0.001. **See also** Figure S5.

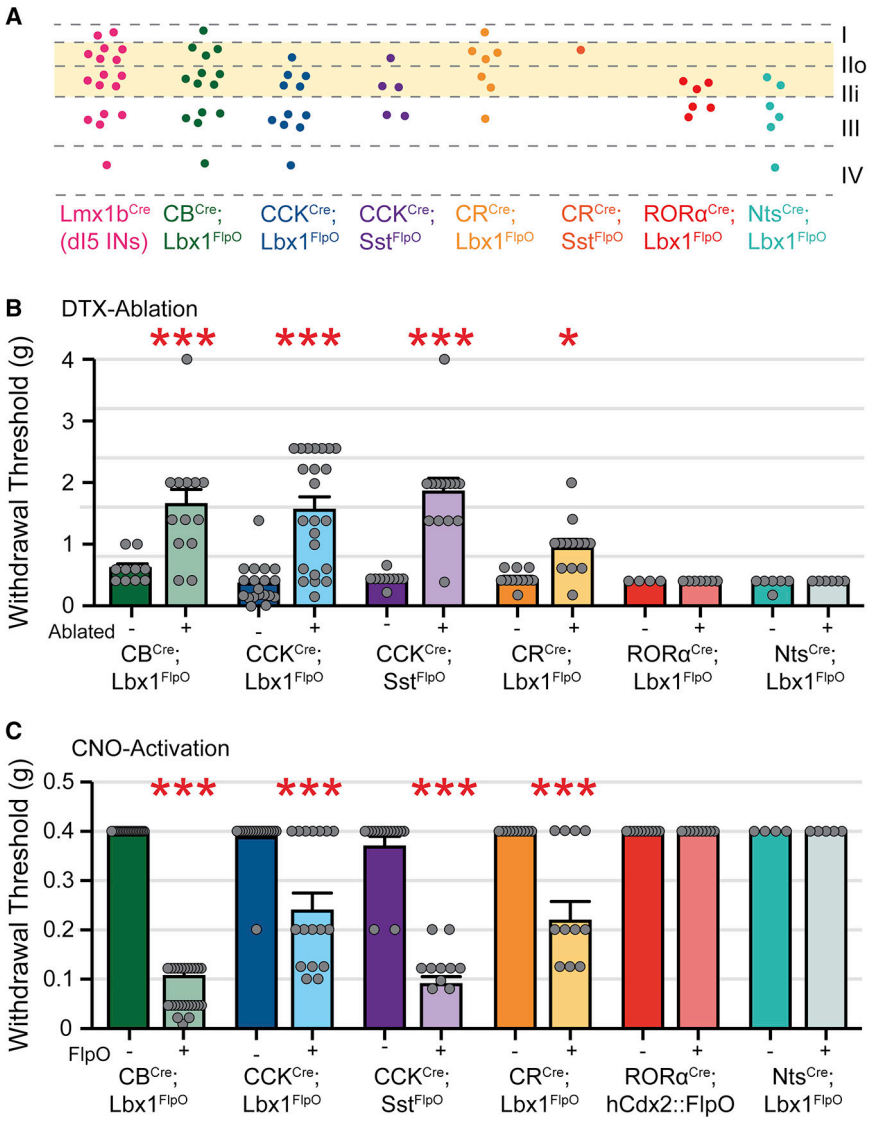

Figure 6. Excitatory INs that span lamina II determine the threshold of mechanical sensitivity

(A) Schematic representation of the distributions of the intersectionally labeled spinal IN populations across the dorsal horn. Each dot represents 20 neurons per 40 μm hemisection.

(B) Increased threshold of paw sensitivity to mechanical stimuli in mice with DTX-induced ablation of CB^{Cre};$Lbx1^{FlpO}$ INs, CCK^{Cre};$Lbx1^{FlpO}$ INs, CCK^{Cre};Sst^{FlpO} INs and CR^{Cre};$Lbx1^{FlpO}$ INs. Controls are either saline-treated *Cre*$^{+}$ and *FlpO*$^{+}$ mice or CCK^{Cre} *FlpO*-negative mice treated with DTX.

(C) Increased sensitivity to von Frey stimulation after CNO-driven neuronal activation in *CB*^{Cre}*;Lbx1*^{FlpO}, *CCK*^{Cre}*;Lbx1*^{FlpO}, *CCK*^{Cre}*;Sst*^{FlpO} and *CR*^{Cre}*; Lbx1*^{FlpO} mice compared to *FlpO*-negative littermate controls, and to *RORα*^{Cre}*;hCdx2::FlpO* and *Nts*^{Cre}*;Lbx1*^{FlpO} mice.

Data are presented as mean ± SEM. Each mouse analyzed is represented with a grey filled circle. Statistical analysis was done using one-way ANOVA followed by Dunnett's post hoc

test comparing all genotypes to $CCK^{Cre};Lbx1^{FlpO-}$ mice, with **p<0.01, ***p<0.001. **See also** Figure S6 **and** Table S1.

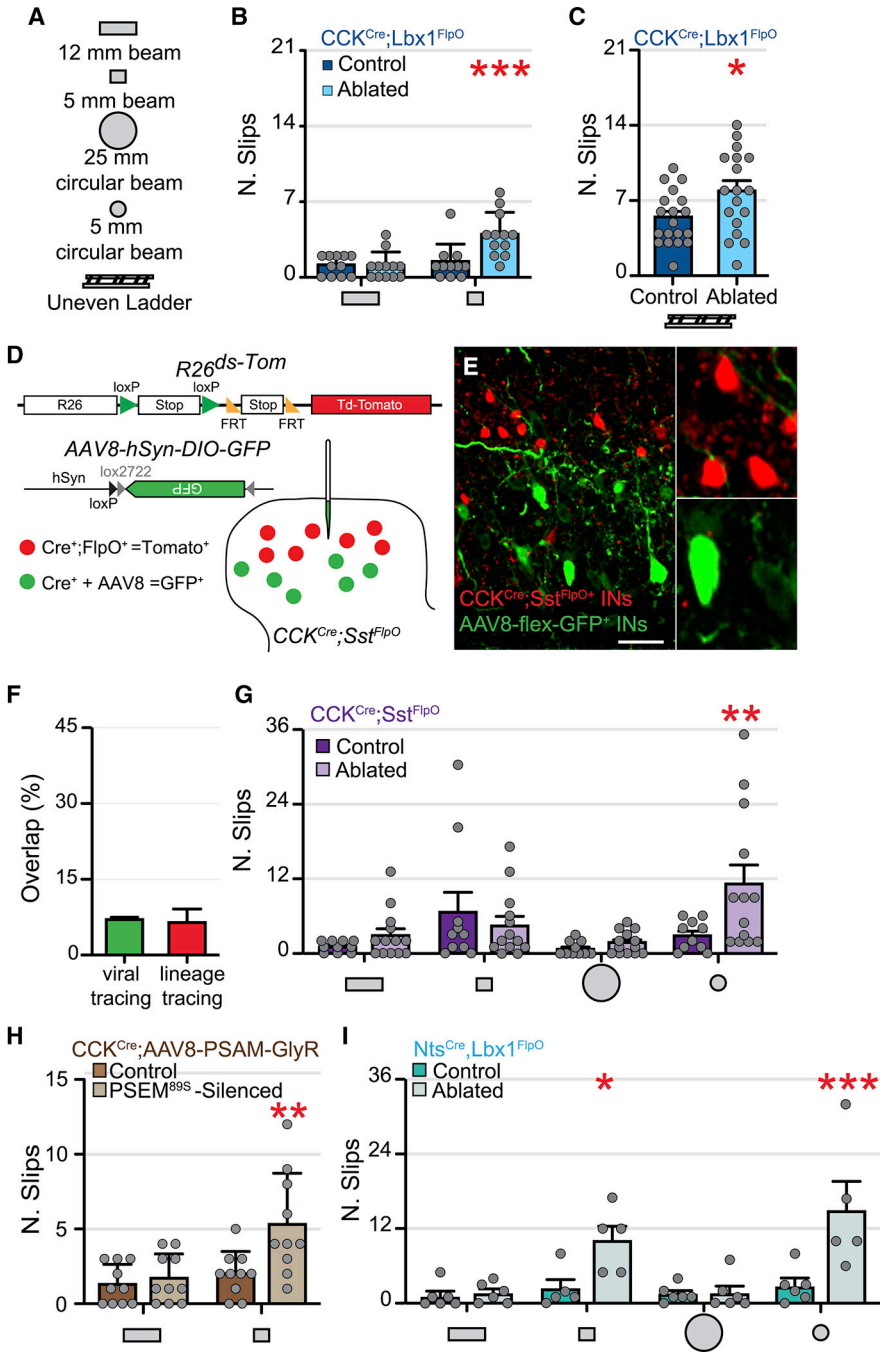

Figure 7. Excitatory neurons in laminae III/IV encode corrective tactile responses

(A) Schematic showing the beam legend for this Figure.

(B,C) Increased number of foot slips following ablation of CCK^{Cre};Lbx1^{FlpO} INs in mice crossing narrow beams (B) or uneven ladder (C). Controls are *FlpO*-negative mice treated with DTX.

(D) Schematic showing the intersectional genetic and viral strategy used to target the superficial (*CCK^{Cre};Sst^{FlpO}*) and deep (AAV8-flex-GFP) subsets of CCK^{Cre} INs.

(E) 30 μm transverse sections through P56 *CCK*^{Cre};*Sst*^{FlpO};*R26*$^{ds\text{-}Tom}$ lumbar dorsal horn transduced with AAV8-flex-GFP and stained with antibodies to Td-Tomato (red) and GFP (green). Scale bar 40 μm.

(F) Graph showing the limited overlap of lineage-traced CCK^{Cre};Sst^{FlpO};R26$^{ds\text{-}Tom}$ INs and AAV-labeled CCK^{Cre} INs compared to the total number of genetically (red bar) or virally (green bar) targeted INs.

(G) Increased number of foot slips on narrow circular beam following ablation of CCK^{Cre};Sst^{FlpO} INs. Control (*Cre*$^{+}$;*FlpO*$^{+}$) mice were treated with saline.

(H) Increased number of foot slips on narrow beam following PSEM^{89S}-induced silencing of *CCK*^{Cre} mice transduced with AAV8-GlyR compared to saline treatment.

(I) Increased number of foot slips during beam crossings following ablation of Nts^{Cre};Lbx1^{FlpO} INs. Control (*Cre*$^{+}$;*FlpO*$^{+}$) mice were treated with saline.

Data are presented as mean ± SEM. Each mouse analyzed is represented with a grey filled circle. Statistical analysis was done using two-way ANOVA followed by Bonferroni's post hoc test, with *p<0.05, **p<0.01 and ***p<0.001. **See also** Figure S7 **and** Table S1.

KEY RESOURCES TABLE

REAGENT or RESOURCE	SOURCE	IDENTIFIER
Antibodies		
Mouse Arc (1:100)	Santa Cruz	Cat# sc-17839, RRID: AB_626696
Rabbit Calbindin (1:250)	Swant	Cat# CB38, RRID:AB_2721225
Rabbit Calretinin (1:250)	Swant	Cat# CR7697, RRID:AB_2619710
Rabbit c-Fos (1:500)	Santa Cruz	Cat# sc-52, RRID:AB_2106783
Sheep CGRP (1:1000)	Abcam	Cat# ab22560, RRID:AB_725809
Goat ChAT (1:50)	Millipore	Cat# AB144P, RRID:AB_2079751
Guinea Pig cMaf (1:5000)	(Wende et al., 2012)	N/A
Rabbit dsRed (1:1000) (anti-Td-Tomato)	Takara Bio	Cat# 632392, RRID:AB_2801258)
Chicken GFP (1:1000)	Aves Labs INC	Cat# GFP-1020, RRID:AB_10000240
Chicken LacZ (1:1000)	Abcam	Cat# ab9361, RRID:AB_307210
Guinea Pig Lmx1b (1:10000)	This paper	N/A
Rabbit NF200 (1:1000)	Sigma	Cat# N4142, RRID:AB_477272
Rabbit Parvalbumin (1:1000)	Swant	Cat# PV27, RRID:AB_2631173
Rabbit Pax2 (1:1000)	Thermo Fisher Scientific	Cat# 71-6000, RRID:AB_2533990
Guinea Pig PKCγ (1:1000)	Frontier Institute	Cat# PKCg-GP, RRID:AB_2571826
Rat RFP (1:1000)	ChromoTek	at# 5f8-100, RRID:AB_2336064
Rabbit RORα (1:100)	Santa Cruz	Cat# sc-28612, RRID:AB_2180141
Goat TrkC (1:1000)	R&D Systems	Cat# AF1404, RRID:AB_2155412
Guinea Pig VGluT2 (1:1000)	Millipore	Cat# AB2251, RRID:AB_1587626
RNAScope Probes		
Mm-Grp	Advanced Cell Diagnostics	Cat# 317861
Mm-Grpr-C2	Advanced Cell Diagnostics	Cat# 317871-C2
Td-Tomato-C3	Advanced Cell Diagnostics	Cat# 317041-C3
Chemicals, Peptides, and Recombinant Proteins		
Blank-Saporin	Advanced Targeting System	Cat# IT-21
Bombesin-saporin	Advanced Targeting System	Cat# IT-40
Chloroquine	Sigma	Cat# C6628
Clozapine N-oxide (CNO)	Sigma	Cat# C0832
Diphteria Toxin (DTX)	List Biological Lab	Cat# 150
Histamine	Sigma	Cat# H7125
PSEM^{89S}	R&D System	Cat# 6426/5
Saline Solution	APP Pharmaceuticals	Cat# NDC63323-186-10
Experimental Models: Organisms/Strains		
Mouse: *Calbindin^{Cre} (CB^{Cre})*	Jackson Laboratory	RRID:IMSR_JAX:028532
Mouse: *Calretinin^{Cre} (CR^{Cre})*	Jackson Laboratory	RRID:IMSR_JAX:010774
Mouse: *Cholecystokinin^{Cre} (CCK^{Cre})*	Jackson Laboratory	RRID:IMSR_JAX:012706

REAGENT or RESOURCE	SOURCE	IDENTIFIER
Mouse: *Chox10::CFP (Chx10^{CFP})*	(Crone et al., 2008)	N/A
Mouse: *hCdx2::FlpO*	(Bourane et al., 2015a)	N/A
Mouse: *Lbx1^{FlpO}*	(Duan et al., 2014)	N/A
Mouse: *Nts^{Cre}*	Jackson Laboratory	RRID:IMSR_JAX:017525
Mouse: *R26$^{Ai14\text{-}Td\text{-}Tomato}$*	Jackson Laboratory	RRID:IMSR_JAX:007914
Mouse: *R26$^{Ai65\text{-}ds\text{-}Td\text{-}Tomato}$*	Jackson Laboratory	RRID:IMSR_JAX:021875
Mouse: *R26$^{ds\text{-}hM3d}$*	Jackson Laboratory	RRID:IMSR_JAX:026942
Mouse: *R26$^{ds\text{-}hM4d}$*	(Bourane et al., 2015b)	N/A
Mouse: *R26$^{ds\text{-}HTB}$*	(Stam et al., 2012)	N/A
Mouse: *RORα^{Cre}*	(Chou et al., 2013)	N/A
Mouse: *Sst^{FlpO}*	Jackson Laboratory	RRID:IMSR_JAX:028579
Mouse: *Tau$^{ds\text{-}DTR}$*	(Duan et al., 2014)	N/A
Virus		
AAV2/1-hSyn-DIO-Synaptophysin::phTomato (1.6×10^{12} vg/ml)	Salk Viral Core	N/A
AAV8-hSyn-DiO-eGFP (4.9×10^{12} vg/ml)	UNC vector core (Chapel Hill, NC)	N/A
hSyn-Flex-rev-PSAM^{L141F}-GlyR-IRES-eGFP (7×10^{12} vg/ml)	UNC vector core (Chapel Hill, NC)	N/A
SADB19-ΔG-mCherry (EnvA) (3.3×10^{10} vg/ml)	Janelia Viral Core (HHMI)	N/A
Software and Algorithms		
Adobe Illustrator and Photoshop Suite	Adobe	www.adobe.com
Excel – Office 2018	Microsoft	www.microsoft.com
Image J	NIH	imagej.nih.gov/ij
Prism	GraphPad	www.graphpad.com
R	The R project	r-project.org